CHALMERS
UNIVERSITY OF TECHNOLOGY

On the estimation of Diesel Particulate Filter Particulate Load based on Pressure Difference

Master's thesis in Mobility Engineering

SAYID ACHMAD MUNTHAHAR

CHALMERS UNIVERSITY OF TECHNOLOGY
Gothenburg, Sweden 2024
www.chalmers.se

Master's thesis 2024

On the Estimation of Diesel Particulate Filter Load Based on Pressure Difference

SAYID ACHMAD MUNTHAHAR
sayid@chalmers.se

CHALMERS
UNIVERSITY OF TECHNOLOGY

Department of Mechanical and Maritime Sciences
Mobility Engineering
Energy Conversion and Propulsion Systems
Chalmers University of Technology
Gothenburg, Sweden 2024

A thesis report submitted as a partial fulfilment for a degree of Master in Science

Supervisors:
Jonas Sjöblom, Chalmers University of Technology
Marco L. Della Vedova, Chalmers University of Technology.
Athanasios Papageorgiou, Scania AB
Examiner:
Jonas Sjöblom, Chalmers University of Technology

Master's Thesis 2024
Department of Mechanical and Maritime Sciences
Mobility Engineering
Chalmers University of Technology
SE-412 96 Gothenburg
Telephone +46 31 772 1000

Typeset in LaTeX
Printed by Chalmers Reproservice
Gothenburg, Sweden 2024

On the Estimation of Diesel Particulate Filter Particulate Load
Based on Pressure Difference
SAYID ACHMAD MUNTHAHAR
Department of Mechanical and Maritime Sciences
Chalmers University of Technology

Abstract

Stricter particulate emission regulations have led to the use of Diesel Particulate Filters (DPF), which is one of the exhaust aftertreatment systems utilized to capture engine-out particulates. However, as particulates accumulate within the DPF, the exhaust pressure drop increases which in turn decreases the overall powertrain efficiency. This necessitates an estimation of particulate load for effective regeneration control–a process to oxidize the soot deposits. This thesis evaluates pressure drop-based particulate load estimation by utilizing recursive Least Squares method to estimate the normalized pressure drop. The study reveals the challenges in achieving high accuracy due to the complex nature of the micro-characteristics of the particulates. Moreover, the author explores alternative applications for pressure difference sensors beyond direct particulate load estimation.

Keywords: Heavy-duty vehicle emission, Particulate emission, Diesel Particulate Filter (DPF), Particulate load estimation, Exhaust aftertreatment system.

Acknowledgements

While I believe this thesis might not even introduce a considerable "dent" to our knowledge, this thesis has tested my capability to explore and learn something new. I will be glad to listen to any feedback from those who I worked with during this thesis as well as the ones who read this report.
First and foremost, I would like to give my greatest gratitude towards my family, especially my parents who have given me endless support. I would not have reached this stage of life without your sacrifices. My warmest appreciation to Amanda, who has given me unwavering support throughout college.
The utmost thanks to Klara and Athanasios who have given me the support, guidance, and opportunity to do this thesis.
I am grateful to have been guided by you Jonas and Marco. Thank you for being very supportive and understanding. I appreciate all the discussions with all the knowledge that you have given to me.
I would like to send my special gratitude to Björn, Magnus, Daniel, Swathy, Saiman, Joakim, Samuel, Srikanth, Giovanna, and everyone I corresponded with in Scania whom I cannot mention all one-by-one for all the fruitful discussions and guidance, be it technical or non-technical. I sincerely wish you the best of luck in your career.

Sayid Achmad Munthahar, Gotebörg-Södertalje, June 2024

Nomenclature

Below is the nomenclature of indices, sets, parameters, and variables that have been used throughout this thesis. Variables which are represented using a hat $\hat{}$ are normalized value to respect confidentiality.

Variables

α	Cell width (m)
β	Forchheimer term (m^{-1})
ΔP_{cake}	Pressure drop due to soot cake layer (Pa)
$\Delta P_{inertial}$	Pressure drop due to inertial effects (Pa)
$\Delta P_{inletchannel}$	Pressure drop due to friction in inlet channel (Pa)
$\Delta P_{outletchannel}$	Pressure drop due to friction in outlet channel (Pa)
ΔP_{tot}	Pressure drop total (Pa)
ΔP_{wall}	Pressure drop due to porous wall (Pa)
ϵ	Error term (Pa)
η	Darcy term in pressure drop normalization ($\frac{s}{m^3}$)
μ	Dynamic viscosity ($kg/(ms)$)
μ_0	Dynamic viscosity term in Sutherland's law ($kg/(ms)$)
ϕ	Q_v μ term in the real-time estimation (kg $\frac{m^3}{s^2}$)
ρ_{soot}	Density of the soot cake layer (kg/m^3)
$\rho_{exhaustgas}$	Density of the exhaust gas (kg/m^3)
θ	Forchheimer term in pressure drop normalization (m^{-4})

ζ	Contraction/expansion inertial losses coefficient
F	Friction factor 28.454 (-)
k_{soot}	Permeability of the soot cake layer (m^2)
K	Kalman gain
k_w	Permeability of the porous wall (m^2)
L	Length of the DPF (m)
$\dot{m}_{exhaustgas}$	Mass flow of the exhaust gas (kg/s))
m_{soot}	Particulate or soot mass (g)
$\dot{m}_{ox}$	Soot oxidation rate (g/s)
N	Number of channels in the DPF
Q_v	Volumetric flow (m^3/s)
R	Covariance matrix in the RLS
S_μ	Sutherland's constant (K)
T_{DPF}	Temperature of the DPF (K)
u_w	Flow velocity (m/s)
V_f	DPF volume (m^3)
w_{soot}	Thickness of the soot cake layer (m)
y	Measured pressure drop in the RLS (Pa)

Contents

List of Figures

List of Tables

1

Introduction

1.1 Background

For decades, heavy-duty vehicles have been critical for inland transport. Most of the heavy-duty vehicles nowadays use compression ignition engine based on diesel fuel. However, this mechanism produces tailpipe emission which has a negative effect to both human health and the environment. One of the most prominent type of diesel tailpipe emission is particulate matter. It has been shown that particulate emission correlates with various health risks involving cancer and pulmonary problems which can be exacerbated into heart attack and stroke as well [1].

Compression ignition engine may produce particulate matter in the form of soluble and insoluble fraction in the form of soot [2]. Soot in general is a solid carbon-hydrogen substance resulted from unburned fuel [2]. Ash particulates coming from fuel additives, lubricants, corrosion and wear particles can also be emitted [3]. Various studies have shown that inhaled particulate matter posses various risks to human health. It is estimated that approximately hundreds of thousands of deaths are related to exposure to particulate matter. Therefore, the amount of particulate matter emitted has to be regulated.

Within European Union (EU), particulate matter tailpipe emission for heavy duty vehicle has been limited by the enforcement of Euro standards. The latest one, Euro VI which was commisioned in 2013, set a strict particulate matter emission standard to under 10 mg per kWh and 6×10^{11} particles per kWh for WHTC cycle [4]. Many techniques are available to reduce engine-out particulate emission. However, with a stricter regulation to comply with, vehicle manufacturers have resorted to the usage of Diesel Particulate Filter (DPF) within the exhaust aftertreatment system. As the name suggests, DPF filters particulate matter coming from the engine by the means of wall-flow filter. Particulate matter in the form of soot and ash get trapped within the DPF walls. This eventually would lead to an increase in exhaust backpressure and reduces the overall efficiency of the powertrain.

One way to clean the DPF is by means of regeneration. in DPF regeneration process,

the soot particles are oxidized by O_2 or NO_2 at a certain high temperature. However, this process cannot be performed continously as it consumes slightly higher fuel to raise the temperature to the suitable one. Therefore, regeneration must be triggered when the amount of soot within the DPF is sufficiently high.
This requires a way to estimate the amount of particulates within the DPF. One of the method is through pressure sensors installed in the inlet and outlet of the DPF. The correlation between the pressure drop and the soot load is utilized to estimate the soot load.

1.2 Purpose

The purpose of the thesis is to evaluate Scania's particulate load estimation by analyzing the available experimental data within Scania with more focus on the pressure drop based estimation. This work can be regarded as a preliminary study if Scania decided to develop the particulate load estimation further. The perspective of this thesis shall be from the point of view of a real-truck driving scenario, in which it cannot be freely assumed that certain variables can be measured unless specified otherwise. Due to the limitation of the thesis, the data considered are the ones that are readily available within Scania's database.

1.3 Scope and Limitations

The scope and limitations of this thesis are as follow:

1. The scope of this thesis is limited to particulate load estimation based on pressure drop measurement.
2. The data is gathered from the existing data within Scania's database.
3. Details regarding the data and hardware are undisclosed and numbers are scaled to respect confidentiality unless specified otherwise.

2

Theory

2.1 Formation of particulate matter in diesel combustion engine

The ignition of fuel in diesel engine relies on spontaneous combustion due to the high temperature and pressure inside the cylinder. Compared to spark ignition engine, the fuel injection sets the timing of the combustion. Typically, this is done right before the piston reaches top dead center such that the combustion occurs during the downward movement of the piston. The flame generated by the combustion can be considered as diffusion flames [5]. The torque produced is then dictated by the amount of fuel injected per cycle [5]. As the fuel-air-ratio within the cylinder increases, soot can be produced if the fuel-air mixing is not perfect and causes locally rich regions within the cylinder. These locally rich regions with correct temperature are the regions in which soot is formed as represented in [6]. It is illustrated in figure 2.1.

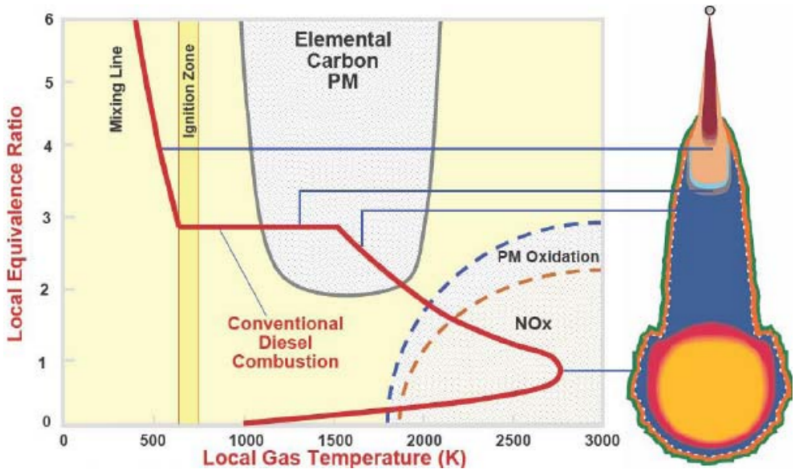

Figure 2.1: The formation of soot and NOx represented in ϕ-T diagram [7].

Soot forms primarily from the carbon element in diesel fuel [5]. While soot formation

in diesel combustion is a complex topic in itself, The widely accepted consensus regarding how the soot is formed is summarized by the following steps [2]: Fuel pyrolisis, nucleation, surface growth, agglomeration, and oxidation. The precursors of soot are produced as a result of fuel pyrolisis which takes the form of unsaturated hydrocarbons, polyacetylenes, polycyclic aromatic hydrocarbons, and acetylene [2]. In the nucleation stage, the soot is transformed from the gas phase into the solid phase in the form of condensed carbon nuclei [8]. This particle will then undergo growth and coalesce which results in an increase in the particle mass without an increase in the number of particles [2, 8]. Collision between the formed soot particles enables those smaller soot particles to agglomerate and form larger soot particles which take the shape of clusters or chains [2, 8]. During the entire formation process, at each stage, some of the particles may become oxidized into combustion products such as carbon monoxide and carbon dioxide [2]. The illustration of the process, as illustrated in [2] is as follows:

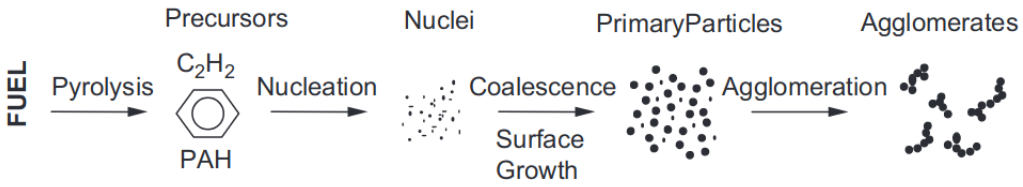

Figure 2.2: Illustration of the soot formation process [2].

Other than soot, particulate matter that can be produced by the combustion process is ash. Ash particles mainly come from fuel additives, lubricants, corrosion and wear particles [3]. Fuel additives that contain metallic elements may produce trace amounts of ash particles after being burned [3]. During engine operations, lubricants may leak into the combustion chamber which causes them to burn. This process contributes to the existence of metallic particles such as Ca, Zn, and Mg in the form of metallic oxides, sulfates, and phosphates. [3, 9]. Micron-sized metallic particles such as iron, chromium, and nickel coming from the corroded and worn-out engine parts may also be included within the engine exhaust as ash particles [3].
The rate of production of ash and soot is in different order. According to this study [9], in a typical medium heavy-duty diesel engine, 386,000 km of driving might typically produce 500 grams of ash, which can be translated into roughly 0,0012 gr/km. Soot, on the other hand, is produced at a much faster rate. Research by Easley et.al in investigating flame temperature effect on soot production gives a value of around 0.15 to 4 grams of soot per kg of fuel burned [10]. Assuming a typical fuel consumption of a heavy-duty truck of 25 l/100 km, this roughly translates to

0,0318 to 0,85 grams of soot per km.

2.2 Particulate Emission Reduction Techniques

Reduction of particulate emission in compression-ignition can be divided into three categories of solutions: fuel, in-cylinder and exhaust aftertreatment.
The structure of the fuel and composition in general affect the soot formation process [2]. The use of oxygenated fuel through ethanol blends will increase the mass fraction of oxygen in the fuel which is shown to reduce the amount of particle emissions [11]. The effect of fuel on soot formation is a complex topic in itself and will not be explained completely within this thesis for the sake of brevity.
In-cylinder solutions involve changing the fuel injection characteristics, mixing aspect, and in-cylinder temperature modifications. Advancing the start-of-injection timing and increasing fuel injection pressure reduces the particulate number because it increases the duration leading to better fuel-air-mixing before start-of-combustion [12]. A small amount of pilot injection also reduces both particulate mass and number [13]. Tree and Svensson in [2] explained that modifications to the shape and geometry of the combustion chamber, characterized by the piston crown, may induce swirling which greatly increases the mixing of fuel and air. By looking at 2.1, better mixing will lower the equivalence ratio therefore avoids the soot formation zone.
Soot formation is also affected by the usage of Exhaust Gas Recirculation (EGR). EGR is a technique that is developed to reduce NOx emission by reducing the in-cylinder combustion temperature. However, EGR usage in general increases soot production as portrayed in the infamous "soot-NOx tradeoff". Figure 2.3 from the work by Dimitriadis et.al in [14] shows the phenomenon.

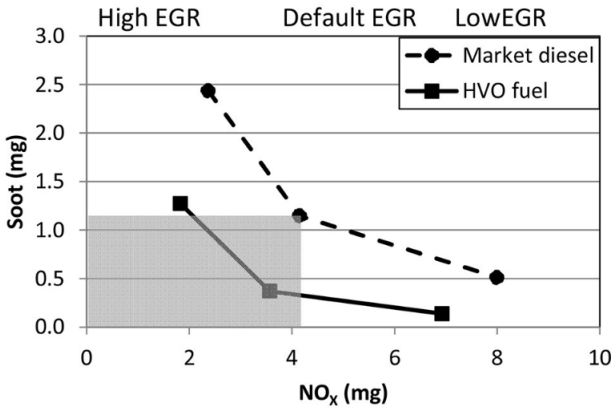

Figure 2.3: Soot-NOx tradeoff [14]

Advanced combustion technologies such as Homogenous Charge Compression Ignition (HCCI), Premixed Charge Compression Ignition (PCCI), and dual-fuel PCCI as studied by Shim et.al in [15] show promising results of both particulate emission and NOx reduction.
However, these efforts alone are not enough to fulfil more recent emission standards. Therefore, an exhaust aftertreatment system specific to reducing particulate tailpipe emission is required.

2.3 Diesel Particulate Filter (DPF)

Diesel Particulate Filter (DPF) is an exhaust aftertreatment device that uses wall-flow monoliths to trap particulate matter. The inlets and outlets are alternatively plugged such that all exhaust gas must pass through the porous wall in which the filtration happens [16]. It is illustrated in the figure below:

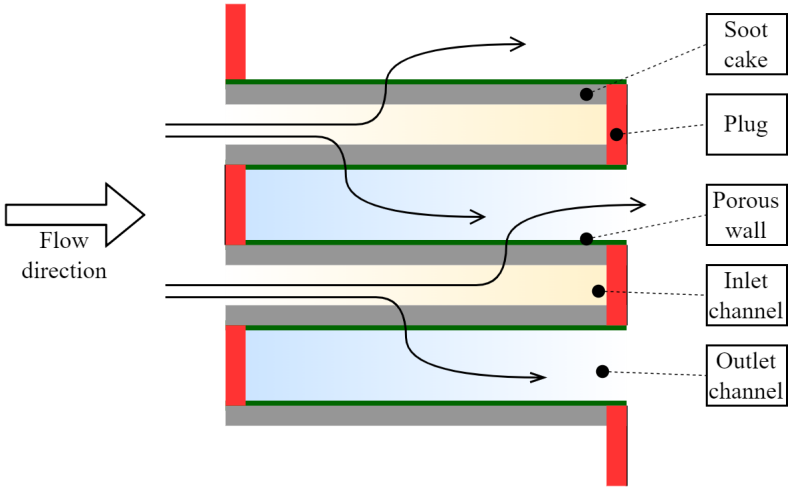

Figure 2.4: Side-view of the DPF filtration process

Trapping of particles are done through six mechanisms: diffusion, interception, inertia, gravity, electrostatics, and thermophoretic. in a DPF, particles are collected within the walls through diffusion, interception, and inertial collection methods [16]. In a clean DPF, soot coming from the engine will be collected within the porous DPF wall. This increases the pressure drop across the DPF as the pores start to fill [17]. The soot particulate layer normally called "soot cake" forms within the wall surface as the pores are filled [17]. During this stage, the filtration efficiency, typically defined as the ratio between the particulate emission trapped within the DPF and the particulate coming out of the engine, increases and may reaches approximately close to 100% [17]. Ash can be deposited within the channel wall, much

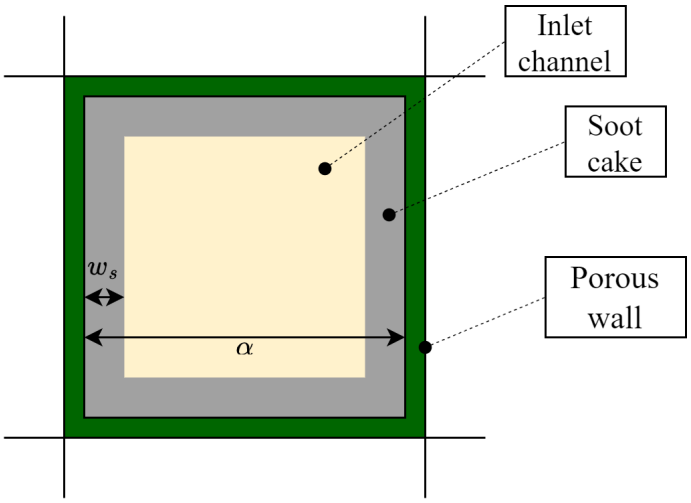

Figure 2.5: Front-view of the DPF inlet channel

like the soot counterpart. However, some observations shown by [18] indicate that ash can be deposited in the end plug of the inlet channel forming the so-called "ash plug" which is illustrated Sappok et.al in [19] as shown in figure 2.6. This is the result of the repositioning of free ash particles such as after regeneration, a process which is explained in the following subchapter. In some cases, ash can also develop an "ash bridge".

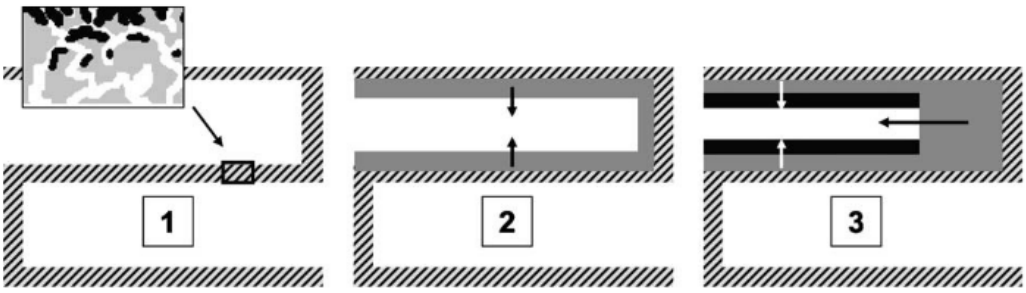

Figure 2.6: Accumulation of Ash as illustrated in [19]
. Ash initially plugs the pores as shown in stage 1. Then, it starts to form a layer within the walls in stage 2. As it grows, it may be re-entrained in the exhaust flow and form a plug-in stage 3 [19]

The pressure drop across the DPF due to particulate load is a matter of interest within DPF development. This is because it will affect the exhaust performance and contribute to an increase in fuel penalty due to backpressure [20].
Konstandopoulos et.al through their work on [21] mentions that pressure drop through a porous filter wall can be modelled as a darcy flow. It is based on Darcy's law which describes the pressure drop of a fluid flowing through a porous medium. It generally has the following form:

$$\Delta P_{darcy} = \frac{\mu}{k} u_w w_w \tag{2.1}$$

Where in this case $_{darcy}$ is the pressure drop through the medium, w_w is the cell width assuming square channel, μ and u are the dynamic viscosity and flow velocity vector respectively, and k is the permeability of the medium. Equation (2.1) essentially expresses that for a flow through porous media, the pressure drop is governed by the viscosity of the flowing fluid, permeability, and the flow velocity itself.

Konstandopoulos et.al in their later work [22] mentions that the Forchheimer effect affects the pressure losses from inertial contributions such as flow contraction and expansion, compressibility effects, and transition to turbulence in the filter channel. It takes the form of [22]:

$$\Delta P_{forchheimer} = \beta \rho {u_w}^2 w_w \tag{2.2}$$

Where in this case $\Delta P_{forchheimer}$ is the pressure drop through the medium, β is the Forchheimer coefficient, ρ is the fluid density, u_w is the flow velocity, and w_w is the cell width. Konstandopoulos et.al and Masoudi et.al through their work in [23, 24] ultimately propose the pressure drop model that takes the darcy-forchheimer form. Stating that the pressure drop within a DPF is a combination of pressure drop components which includes flow through inlet and outlet channel, effects through wall and soot layers, and flow contraction and expansion term. It is mathematically expressed through the following equation:

$$\Delta P_{tot} = \Delta P_{wall} + \Delta P_{inletchannel} + \Delta P_{outletchannel} + \Delta P_{cake} + \Delta P_{inertial} \tag{2.3}$$

Where:

$$\Delta P_{wall} = \frac{Q_v \mu}{2V_f} (\alpha + w_w)^2 \left[\frac{w_w}{k_w \alpha}\right] \tag{2.4}$$

$$\Delta P_{inletchannel} = \frac{Q_v \mu}{2V_f} (\alpha + w_w)^2 \left[\frac{4FL^2}{3} \frac{1}{(a - 2w_{soot})^4}\right] \tag{2.5}$$

$$\Delta P_{outletchannel} = \frac{Q_v \mu}{2V_f} (\alpha + w_w)^2 \left[\frac{4FL^2}{3} \frac{1}{a^4}\right] \tag{2.6}$$

$$\Delta P_{cake} = \frac{Q_v \mu}{2V_f} (\alpha + w_w)^2 \left[\frac{1}{2k_{soot}} ln\left(\frac{\alpha}{\alpha - 2w_{soot}}\right)\right] \tag{2.7}$$

$$\Delta P_{inertial} = + \frac{\rho Q_v^2 (\alpha + w_w)^4}{V_f^2 \alpha^2} \left[\frac{\beta w_w}{4} + 2\zeta(\frac{L}{\alpha^2})\right] \tag{2.8}$$

Hence:

$$\Delta P_{tot} = \frac{Q_v \mu}{2V_f}(\alpha + w_w)^2 \left[\frac{w_w}{k_w \alpha} + \frac{1}{2k_{soot}} ln\left(\frac{\alpha}{\alpha - 2w_{soot}}\right) + \frac{4FL^2}{3}\left[\frac{1}{(a - 2w_{soot})^4} + \frac{1}{\alpha^4}\right]\right] + \frac{\rho Q_v^2 (\alpha + w_w)^4}{V_f^2 \alpha^2}\left[\frac{\beta w_w}{4} + 2\zeta(\frac{L}{\alpha^2})\right] \quad (2.9)$$

Where the soot is assumed to be deposited as a uniform cake layer throughout the inlet channel and the mass can be estimated a geometrical relation expressed by:

$$m_{soot} = \left[\alpha^2 L - (\alpha - 2w_{soot})^2 L\right] \rho_{soot} N \quad (2.10)$$

It should be noted that the pressure drop is defined as positive when the pressure downstream of the DPF is lower than upstream. In a clean DPF, no pressure drop is coming from the soot cake layer term. Then particulates start to deposit within the porous wall, causing the decrease in the wall permeability k_w [25]. When the soot cake layer develops, w_{soot} starts to increase and further increase the pressure drop.

There are multiple models of DPF pressure drop. Aligned with what Depcik et.al in [26] have observed, similarities exist within the equations. The general trend is that the model contains Darcian and Forchheimer effects through the wall and soot layers, inlet and outlet channel losses, and contraction and expansion losses, much like the model in (2.9) [26]. Some may also extend the models to include soot plugs, ash accumulation, and asymmetric channel sizes [26].

To reduce the fuel penalty due to pressure drop, DPF needs to be cleaned regularly with a mechanism normally called "regeneration" during which the soot particles are oxidized. Ash, however, cannot be oxidized with this method [20]. The main idea of regeneration is to oxidize the carbonaceous particles inside the DPF into carbon dioxide. This can happen through reacting with oxygen and/or nitrogen oxide. The reaction might take multiple steps [27]. The reaction itself is a complex process and will not be described in detail within this thesis for brevity.

This oxidation process however only happens when the right temperature is met. Oxygen-based regeneration requires higher DPF temperature which is around 600°C [3]. This temperature, however, is not a typical temperature of the diesel engine exhaust except during active regeneration. Nitrogen oxide-based regeneration can happen at lower temperatures provided enough Nitrogen oxide concentration is available [3]. This is supported by catalyst which oxidizes NO to NO_2

The regeneration process without a deliberate attempt to increase DPF temperature

is called passive regeneration. One way to achieve this is through coating the DPF with catalysts such as Pt, Ce, or Cu to lower the activation energy required for the reaction to happen[3]. This Catalyzed DPF (CDPF) is therefore capable of oxidizing soot deposits in lower temperatures, typically around 300-400°C. Another way to promote passive regeneration is through the usage of Continuously Regenerative Trap (CRT) [3]. in a CRT system, Diesel Oxidation Catalyst (DOC) is used to oxidize nitrogen monoxide, among others, to increase the concentration of nitrogen oxide before the flow goes to the DPF [27]. When there is a substantial amount of soot within the DPF while the temperature does not promote oxidation reactions, active regeneration is performed. There are several examples of usage of auxiliary systems to increase the temperature of the DPF such as by using flame burner, electric heater, microwave heater, and non-thermal plasma [3]. However, there are also methods to increase the DPF temperature by means of engine control such as by performing one or two post-injections, intake throttle closure, turning off exhaust gas recirculation, and keeping turbocharger open [3]. For conciseness, the details of the aforementioned active regeneration mechanism will not be discussed in this thesis.

The regeneration process requires careful control due to two reasons: regeneration reduces fuel efficiency and uncontrolled regeneration may reduce DPF service life [28]. The reduction in DPF service life may occur if thermal runaway within the DPF happens. If the exhaust flow suddenly drops during active regeneration, the exhaust flow may contain high oxygen concentration while some amount of particles are in the light-off state and unoxidized yet [28]. This drop-to-idle phenomenon may cause a sudden increase in DPF temperature especially if the soot loading is high. [28].

Therefore, estimation of the particulate loading in the DPF is required to initiate and control the regeneration process to achieve the best efficiency.

2.4 Soot Load Estimation

Estimation of DPF soot load is a challenging task since essentially direct soot load measurements are mostly done at the laboratory stage and not economical for commercial operations as mentioned in [29, 30]. In general, according to the author's current knowledge, There are in general two main methods of estimating soot load: model-based and pressure-difference-based. Model-based estimation relies on careful modelling of processes within the DPF and soot generation. It mainly uses the following basic assumption: soot deposit within the DPF is the collected soot sub-

tracted from the amount oxidized. The model is then extended to include filtration modelling to include the evolution of filtering efficiencies. A more detailed review of model-based estimations can be seen in the work by Yan et.al [29]. Pressure-difference based is as the name suggests, based on the difference of the static pressure between the DPF inlet and outlet (pressure drop). Accumulation of particles within the DPF causes an increase in pressure drop. Therefore, the relation between pressure drop and particulate load can be inferred. Some models mixed both of the approaches such as in [31, 32].
The calibration map in this case serves as the basis for estimating soot mass from pressure drop in the default estimation. It is constructed by a calibration process in which the detail is not explained to respect confidentiality. The map can be plotted in the following figure:

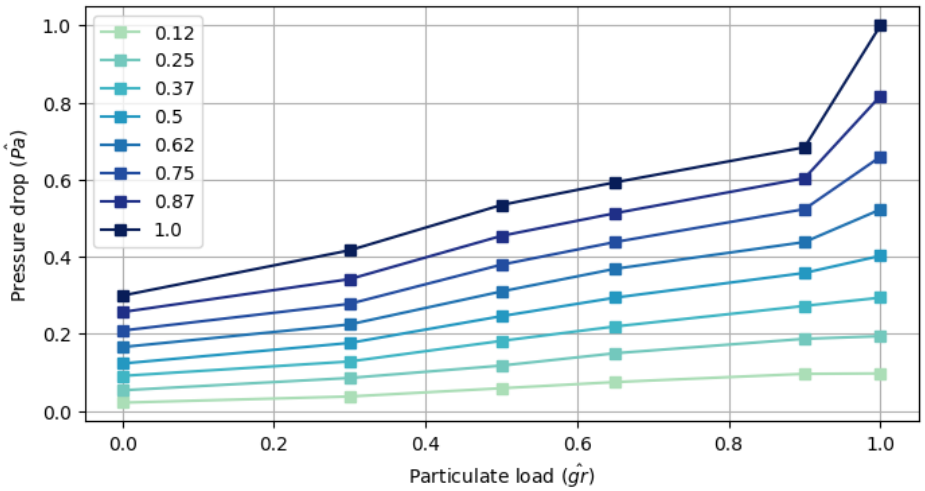

Figure 2.7: Default estimation calibration map

This map is essentially "particulate load" so there is no differentiation between soot with different compositions, nor differentiation between soot and ash particulates. In fact, the response of the pressure drop with respect to particulate load is different between soot and ash. The soot effect to the pressure drop is more commonly observed in various literatures and some examples can be seen in figure 4.5 and 4.6. The effect of ash to pressure drop highly depends on how the ash is deposited and distributed within the DPF. Observations by Sappok et.al in [9, 33, 34] and Singh in [35] show that ash deposits affect the sensitivity of the pressure drop with respect to soot load and conversely, soot distribution and regeneration approach affects how the ash is distributed within the wall.
Scania uses a mix of both approaches albeit in a parallel way. The pressure drop-based approach relies on a static calibration map of volumetric flow, pressure drop,

and soot mass combined in series with an undisclosed algorithm. From this point on, this estimation model is referred as the default estimation model. Further details regarding the methods are omitted to respect the classified nature of this item. Furthermore, variables represented with a hat ""$arenormalizedduetotheaforementionedreason$.

3

Experimental Data for Evaluation

3.1 Normalization of pressure drop

Readings of pressure drop across a DPF are heavily affected by the volumetric flow velocity as shown in the (2.9). Therefore, it is practical to normalize the pressure drop concerning flow velocity and viscosity to remove the effect of flow velocity and viscosity. This approach uses a different meaning of "normalization" as it does not produce a unit-less value. This principle is also done in other references such as [36] Equation (2.9) can be written in the following form:

$$\Delta P_{DPF} = \eta(Q_v\mu) + \theta(Q_v^2\rho) \tag{3.1}$$

Where η and θ represent the variables in the Darcy term and Forchheimer term as in the equation (2.9) respectively.
η comprises the pressure drop effects due to Darcian effects with parameters such as soot permeability, wall permeability, soot cake thickness, and the geometry of the DPF. θ is a term related to the inertial effect of the flow. The second term, however, can be neglected to simplify the empirical equation. This argument can also be found in [37]. Other references such as [31, 38] showed that the contribution of inertial effects to the pressure drop is roughly less than 10% of the total pressure drop. It is also noted that in this work, the aftertreatment system involves no compression and expansion channel in the inlet and outlet of the DPF respectively. The pressure sensor is also located right on the inlet and outlet the DPF. Therefore, it is safe to neglect the inertial term in this work and the equation is assumed to be:

$$\Delta P_{DPF} = \eta(Q_v\mu) \tag{3.2}$$

Equation (3.2) has a linear form. Therefore, regression approaches can be performed to estimate η provided that the measurements of ΔP_{DPF}, Q_v, and μ are also available.
While μ cannot be measured directly, it can be estimated by the Sutherland's law:

$$\mu = \left[(\frac{T_{DPF}}{T_0})^{\frac{3}{2}} \left(\frac{T_0 + S_\mu}{T_{DPF} + S_\mu} \right) \right] \mu_0 \tag{3.3}$$

In this thesis, it is assumed that the pressure of the air within the DPF is the same as the DPF temperature. The constants μ_0 and S_μ are based on air.
One can estimate the value of η by performing an ordinary least squares regression. However, it would not be practical for real-time estimation. As discussed in Appendix 1. With a real-time estimation method in mind, The value of η can be estimated by Recursive Least Squares (RLS) method. As mentioned in [39], RLS is an online identification method that produces estimates of a time-varying parameter at time t based on information from time $t-1$. This approach is used to ensure the applicability of this method in real driving situations. In this thesis, The RLS algorithm that is used is based on [39]. Mathematically, the system can be expressed as:

$$y(t) = \eta \phi^T(t) \tag{3.4}$$

By applying the principle of Kalman filter and modelling the parameter as time-varying with random walk or drift, the parameter can be estimated with the following algorithm:

$$\begin{aligned} \eta(t) &= \eta(t-1) + K(t)\epsilon(t) \\ \epsilon(t) &= y(t) - \phi^T(t)\eta(t-1) \\ K(t) &= P(t-1)\phi(t) / \left[1 + \phi^T(t)P(t-1)\phi(t)\right] \\ P(t) &= P(t-1) - P(t-1)\phi(t)\phi^T(t)P(t-1) / \left[1 + \phi^T(t)P(t-1)\phi\right] + R \end{aligned} \tag{3.5}$$

The new estimate of η is simply a multiplication of the error term ϵ by a gain K which is based on the covariance matrix P and the measurements of ϕ. The matrix R determines the ability to track time variations with larger R giving more aggresive variations [39]. Hence, tuning the value of R is a matter of determining how the estimator will behave. A more detailed explanation regarding RLS can be seen in [39, 40].
The update policy of RLS is also something to consider. A very relaxed RLS tends to be relatively noisy. In this thesis, the value of η is updated when the volumetric flow across the DPF is more than 100 liter/second. This is further discussed in Appendix 1.

3.2 Experimental Setup

The experiments were done with an engine and aftertreatment system with the following specification:

Table 3.1: Specification of the engine and aftertreatment system used in the experiment

Number of cylinders	6
Displacement	13 L
Power rating	370 hp
EGR	No
DOC	No

Further details regarding the engine and aftertreatment system are omitted to respect confidentiality. The data evaluated is coming from DPF testings which ran multiple sets of heavy-duty Federal Test Procedure (FTP) which represents the high-load regime and a bespoke Low-Load Cycle (LLC) which represents the low-load regime. Utilizing driving cycles would approximate real driving situations better compared to constant flow experiments. These cycles are repeated to load the DPF with particulates. After a certain amount of cycles, the DPF is taken off and weighed in a temperature of 200°C to prevent moisture from contaminating the weights of the particulates and consistencies between measurements. The weights are then subtracted by the empty DPF weights to obtain the weights of deposited particulates. The plot of the engine speed and torque response for each cycle is plotted below:

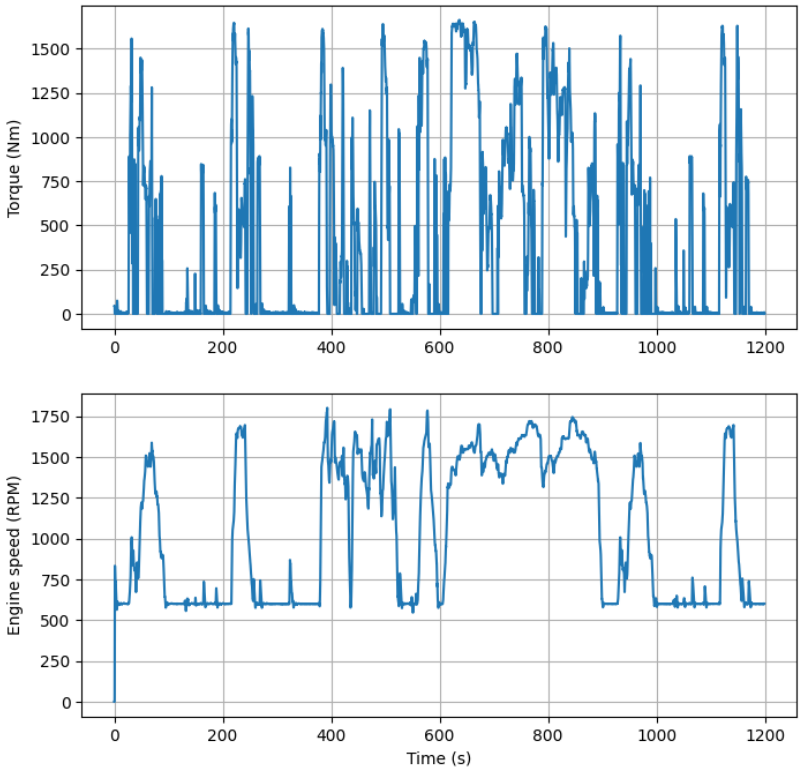

Figure 3.1: Torque and RPM response in FTP case

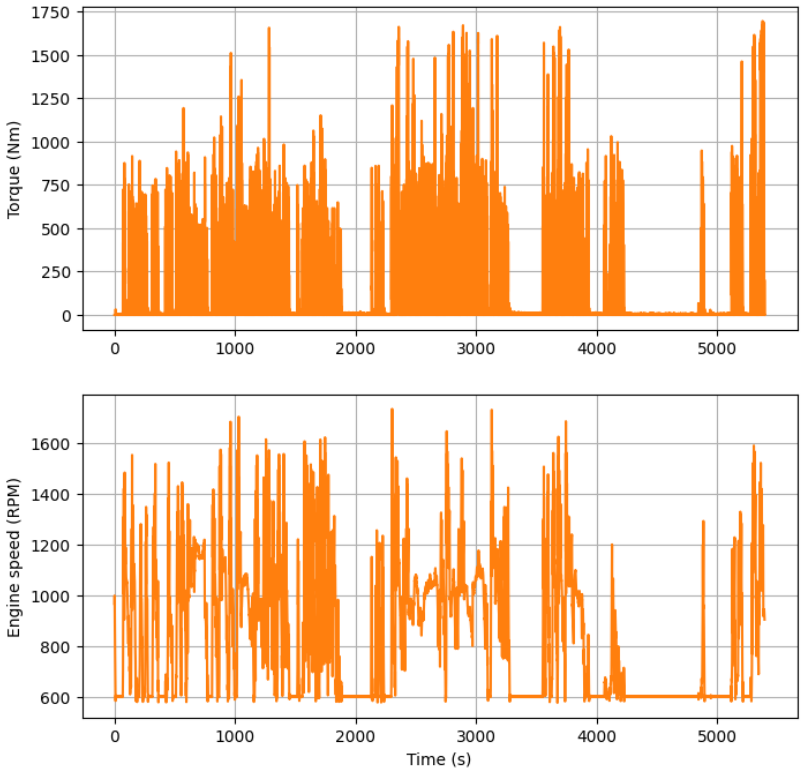

Figure 3.2: Torque and RPM response in LLC case

As the name suggests, LLC contains a lower load compared to the FTP. The average power in a single FTP in this case is 55.3 kW while it is 18.7 kW for LLC. During testing, there are cases where the engine performs engine braking, indicated by negative torque. However, in this analysis, the negative torques are saturated to zero torque.

FTP loading cycles are done for 60 loops with DPF weighings at the 31th, 55th, and 60th loops. There are 109 loops in the LLC loading case, with DPF weighings at 25th, 35th, 51st,64th, and 109th cycle. However, starting from the 64th cycle and onwards, the engine was run in passive regeneration mode. This mode corresponds to higher exhaust gas temperature and NOx concentration which promotes soot oxidation. nj,8jbpThe regenerative case then consists of the 64th up to 109th LLC cycle. Between the FTP and LLC case as well as at the end of the LLC regeneration case, a deliberate soot burn is performed by exposing the DPF to a high RPM, high torque, and high exhaust gas temperature to completely burn all the soot deposited within the DPF. The effect of ash can be considered negligible and it can be assumed that each set starts with a DPF empty of soot. This is supported by the fact that at the end of the testings, the amount of ash in the DPF is below one gram per litre of DPF volume, which according to the author's knowledge is a very low value for ash to have a profound effect to the pressure drop.

Regarding the default estimation, as mentioned in the previous chapter, it uses a mix of pressure drop-based and model-based estimation. In the FTP loading case, the most used method is the pressure drop-based while the latter is used more in the LLC loading case. The default estimation uses an oxidation model during the regeneration mode. Thus, the default estimation reading is not based on pressure difference during the regenerative modesm j+99.5. However, the pressure difference is still measured during that mode. There is also a condition-checking mechanism which determines whether to use pressure difference-based estimation or engine-out soot estimation. It should be noted that the default estimation estimates soot load instead of both ash and soot load. However, as mentioned in the previous passage, it can be assumed that only soot particulates exist in the DPF for this thesis. The amount of ash accounted in the DPF at the end of the entire test is deemed insignificant for the ash to have an effect on pressure drop. The details are not explained further to respect confidentiality.

In summary, the data that is analyzed consists of the following sequence:

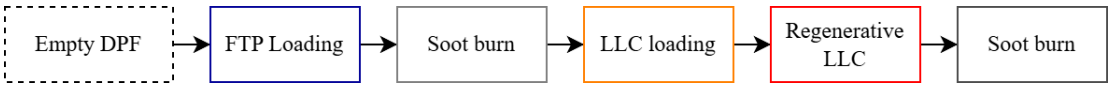

Figure 3.3: The testing sequence

It should be noted that performing these repeated cycles should not always be assumed as a loading-only mode in which the DPF particulate load is monotonically increasing. Soot oxidation might occur simultaneously while the engine is running and producing soot. This argument is also evident in the LLC regenerative case where the engine still produces soot while the amount of soot in the DPF decreases. This can be observed in the next section.

3.3 Results

As mentioned in section 3.2, even though there are two particulate load estimation models used, the pressure difference is still measured regardless of the model used. Therefore the value of η can still be evaluated at every mode. The pressure drop-based estimation model is used only around 10% of the time during LLC cycles.
The real soot mass deposited within the DPF is assumed to be a linear interpolation of the DPF weights measurement. The plot of the default estimation and the interpolated weighed mass are as follow:

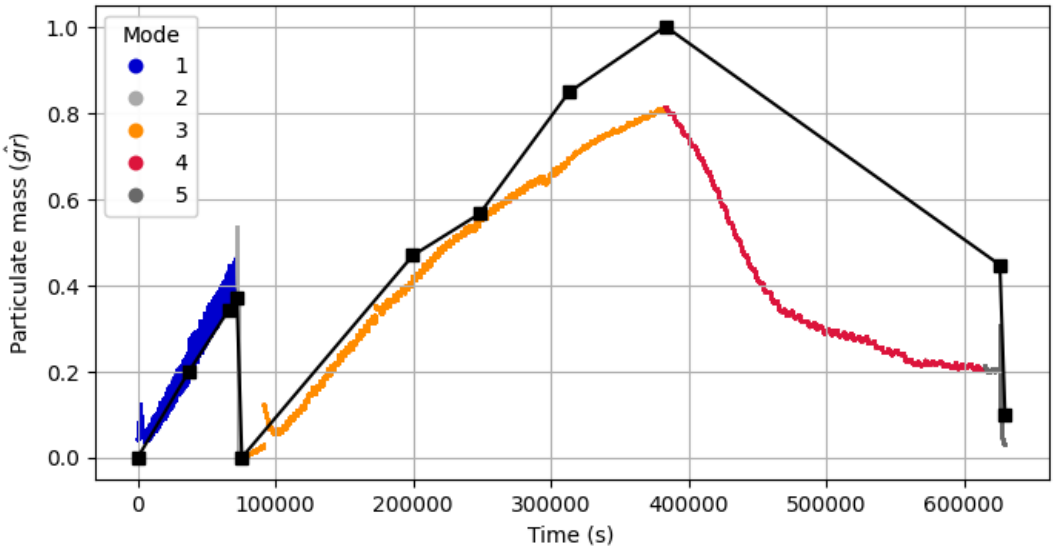

Figure 3.4: The black lines is the particulate mass based on the DPF weighings and the coloured lines are the default estimation coloured based on different modes

Where the modes corresponds to:

Mode	Explanation
1	FTP loading
2	Soot burn post FTP
3	LLC loading
4	Regnerative LLC
5	Soot burn post LLC

Table 3.2: Mode labels with sequence illustrated in 3.3

The is then calculated using the aforementioned method. The plot of η at none-soot burn mode 1,3,(3+4) with respect to the interpolated soot mass are as follows::

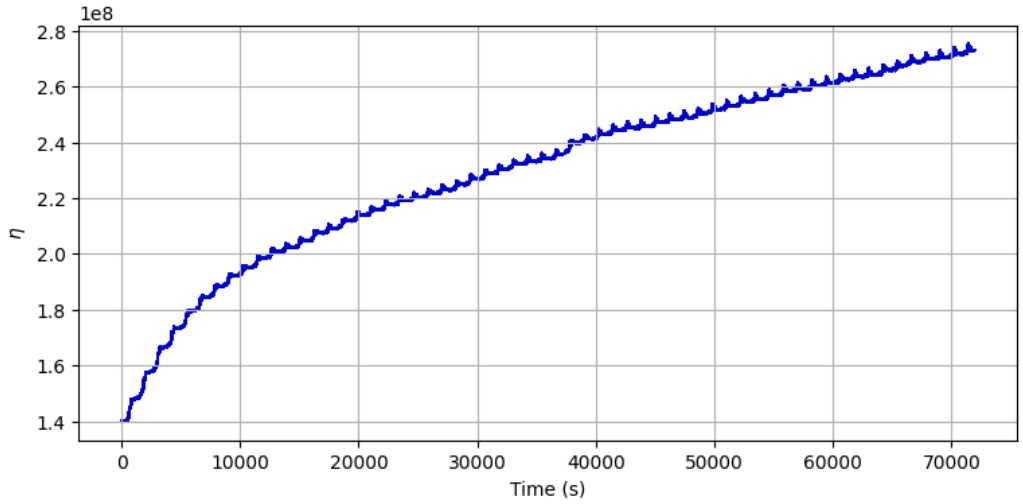

Figure 3.5: η in mode 1

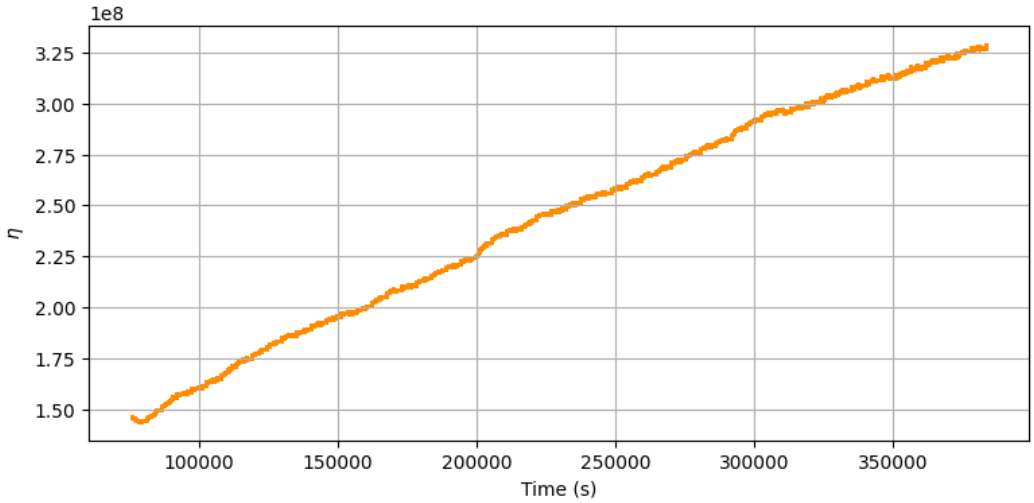

Figure 3.6: η in mode 3

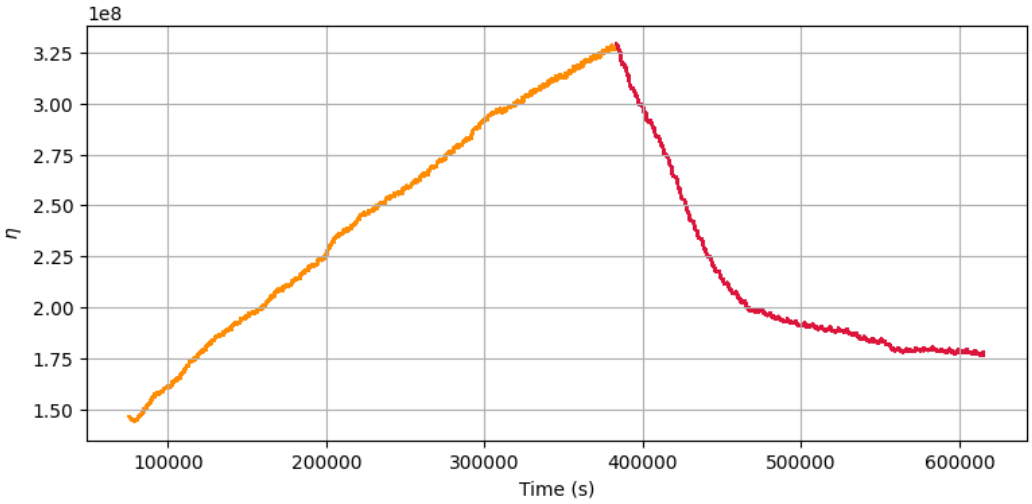

Figure 3.7: η in mode 3-4

We can now plot the evolution of η with respect to the interpolated particulate mass at every modes.

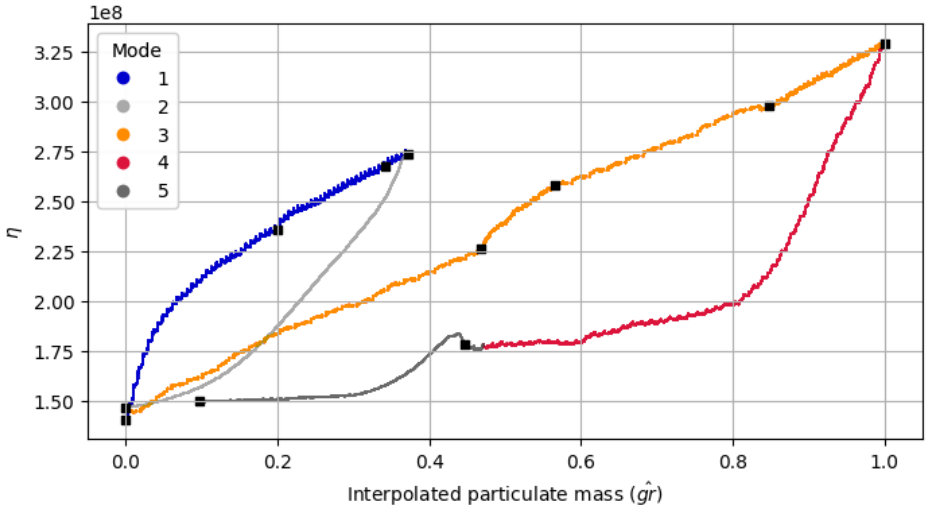

Figure 3.8: The plot of the value of η with respect to the interpolated particulate mass

As we can see visually, η and the default estimation model have a similar shape in general. In the loading cases, they both show increases and in the regenerative case, it decrease. Therefore indicating the existence of information regarding particulate load in η. Figure 3.8 also shows that different conditions of pressure drop might correlate with different particulate mass within the DPF. The next chapter aims to investigate this.

4

Discussion

4.1 Evaluation of the default estimation normalized calibration map

We now perform the normalization of the calibration map shown in figure 2.7. RLS method is not used to normalize this calibration map since the map exist in the form of table. Instead, normalization is done by dividing the pressure drop with the volumetric flow. We will get the same value as η without the viscosity term. Adding a viscosity term to this map would infer that the map will consist of multiple surfaces. Thus, for the sake of brevity, we assume constant viscosity in this case. The plotted map with normalized pressure drop is as follows:

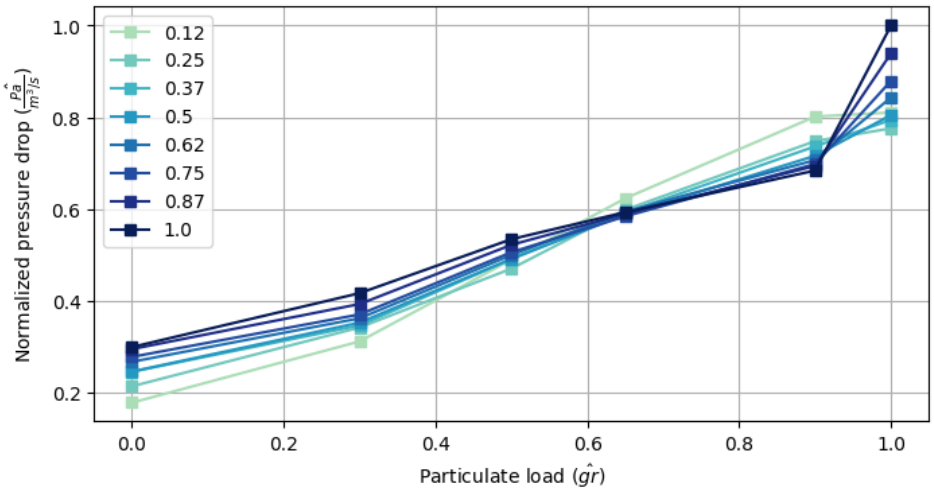

Figure 4.1: Normalized default estimation calibration map

We can observe that the maps do not have a high resolution of the particulate load in low amount of particulate load. It implicitly assumes that the growth of the pressure drop at low particulate load is linear while in fact it is generally non-linear due to the wall filtration process. It is difficult to interpret the phenomenon that this normalized calibration map captures. By evaluating (2.9), the difference

in normalized pressure drop–represented by η–with similar particulate load implies that there are differences that can be attributed to the difference in the soot cake layer permeability k_{soot} and/or the soot cake layer density ρ_{soot} as well as the soot cake thickness w_{soot}. Higher η may imply lower k_{soot} and vice versa. The relation to the density ρ_{soot} and thickness w_s is more complex. Mathematically speaking, higher w_s in equation (2.9) causes higher η. We can think of it as higher cake thickness causing higher pressure drop due to friction. However, with similar mass, it implies that the cake density ρ_{soot} is lower. This particular phenomenon is difficult to verify since several studies such as [23, 41] shows that cake density is coupled with the permeability even though equation (2.9) does not show that.

4.2 Loading cases

The prediction done by the default estimation is plotted together with the interpolated particulate mass in the following figure:

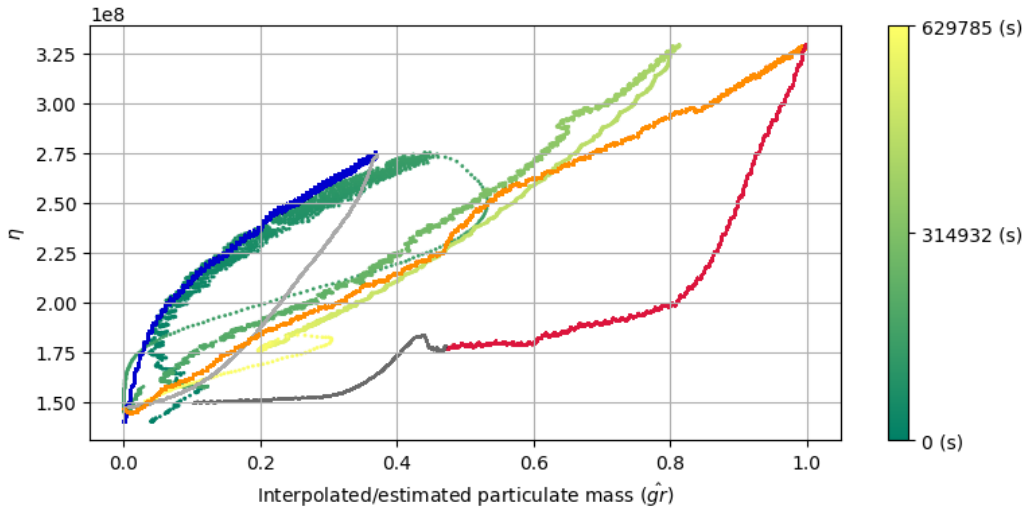

Figure 4.2: This figure compares the prediction done by the default estimation (X-axis) compared to the approximate mass (interpolated mass). The Y-axis shows the normalized pressure drop η at each given predictions.

Reader is advised to refer to figure 3.3 for the temporal aspect and figure 3.8 for the evolution of η with respect to the interpolated particulate mass during different modes to aid in interpreting figure 4.2. This figure compares the default estimator and interpolated particulate mass estimate with the evolution of η in different modes. It visualizes the real particulate mass and the estimates by the default estimator for each η. For clarity, the modes will be discussed separately. This subsection discusses the loading cases.

In figure 4.2, we can see that the default estimation (shown by green-yellow curves) during FTP loading has a good approximation. The default estimation line is relatively "close" to the blue line. The same thing happens in the LLC loading mode. We know that during LLC mode, the estimation is not using the pressure drop-based estimation for the most part. This indicates that the default estimation's switching algorithm performed well. If the pressure-drop-based estimation is used, then the estimate will tend to approach that of the FTP loading case.
The interpolated particulate mass and default estimation of loading mode 1 and 3 are plotted with η in the following figures respectively:

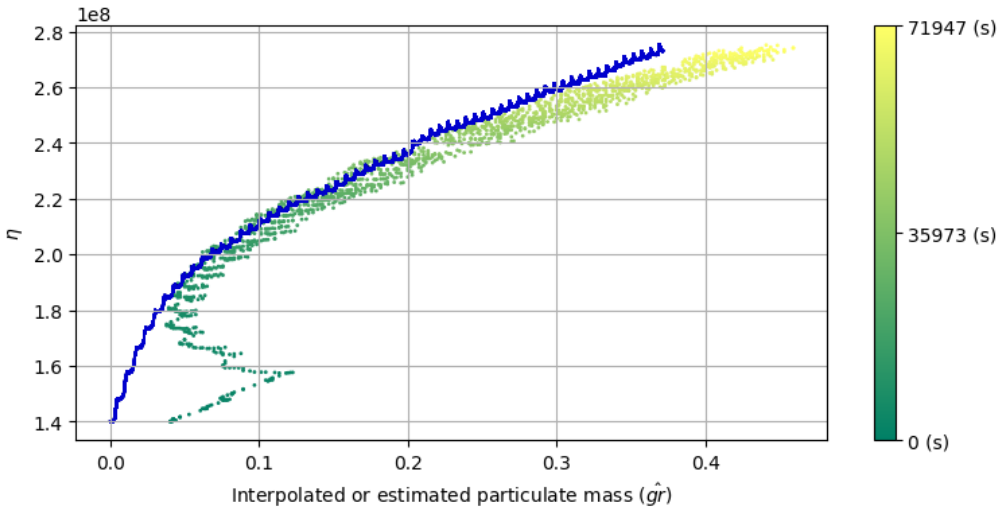

Figure 4.3: This figure compares the prediction done by the default estimation (gradient-colored curve) compared to the approximate mass (blue curve) during FTP loading. The X-axis shows the particulate mass based on the interpolation or default estimation. The Y-axis shows the normalized pressure drop η at each given predictions.

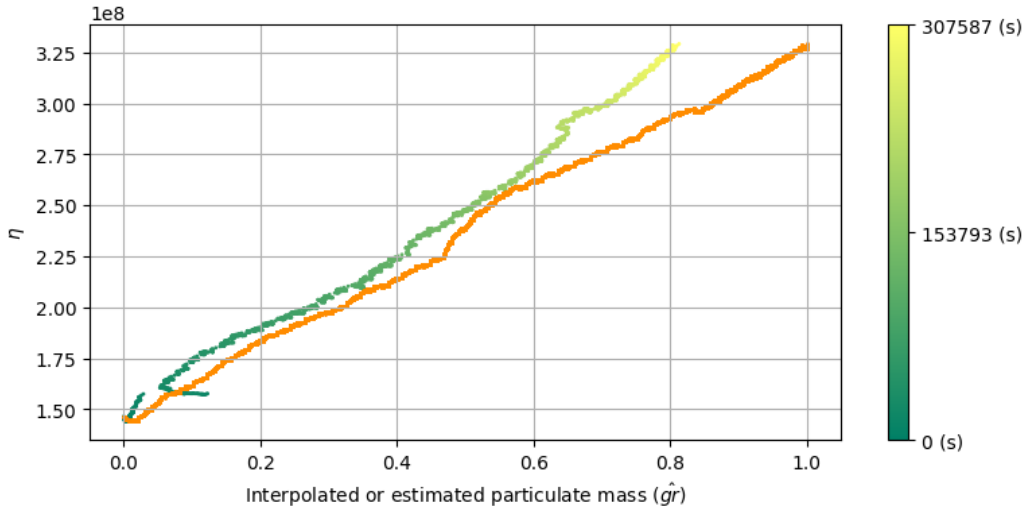

Figure 4.4: This figure compares the prediction done by the default estimation (gradient-colored curve) to the approximate mass (blue curve) during LLC loading. The X-axis shows the particulate mass based on the interpolation or default estimation. The Y-axis shows the normalized pressure drop η at each given prediction

Both figures shows that as the loading progresses, the normalized pressure drop starts to increase. However, in higher pressure drops, the default estimation starts to have offset from the approximated mass in both mode 1 and 3. In mode 1, the default estimation tends to overestimate while in mode 3 it underestimates. However specifically for mode 3, the behavior of default estimation cannot be attributed to the pressure-drop model entirely.

Binning is done to simplify the visualization of the η with respect to the interpolated particulate mass to identify the transition to soot cake filtration. It is performed by aggregating the data into windows of width 1000 seconds for both FTP and LLC and take the average of the η within the window. The results are as follow:

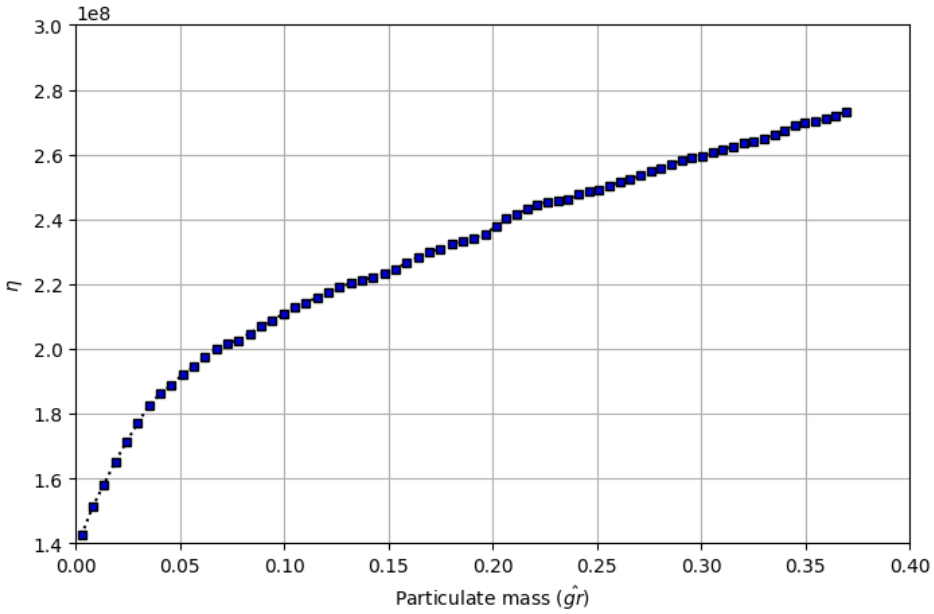

Figure 4.5: Binned η vs mass in FTP case

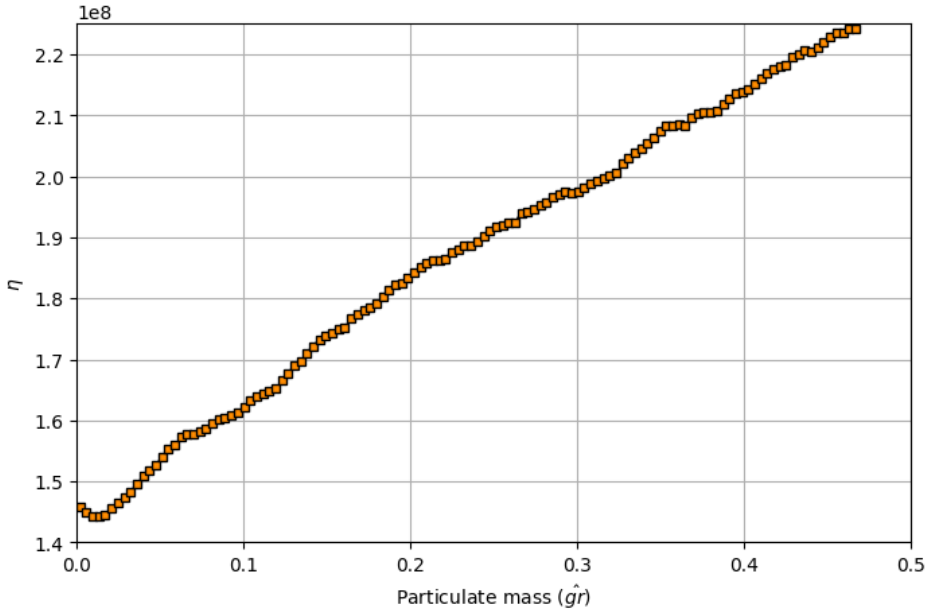

Figure 4.6: Binned η vs mass in LLC case. Note the X-axis is trimmed for clarity

In the binned figures above, the transition from wall filtration to cake filtration can be identified in both cases. In this thesis, the transition is determined manually by observing figures 4.5 and 4.6. Transition is identified by the decrease in pressure drop gradient after the initial phase of the loading as shown in various research regarding DPF such as [37, 42]. The following results can be presented:

Variable	FTP	LLC
Soot cake gradient ($\frac{\eta unit}{\hat{gr}}$)	2.074×10^4	1.288×10^4
Soot mass around cake filtration onset ($\hat{gr}$)	0.06183	0.06233
η around cake filtration onset (η_{unit})	1.98×10^8	1.57×10^8

Table 4.1: Values around the onset of cake filtration

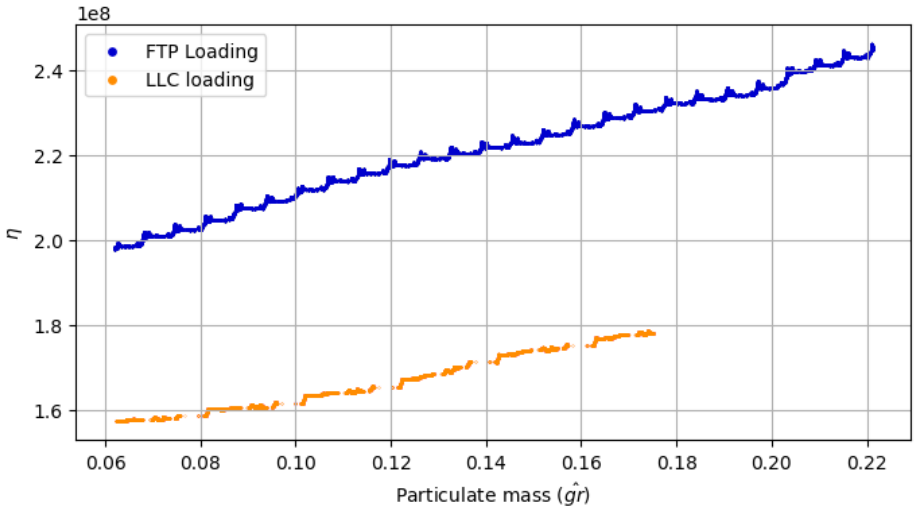

Figure 4.7: η during cake filtration

These results suggest that even though it uses the same engine and exhaust aftertreatment system, a different way of driving would cause different pressure drop behavior with respect to the particulate load. Though both FTP and LLC loading cases have similar values of η at certain points, they correspond to different particulate masses as can be observed in figure 4.2 and 4.7. The gradient can also be different while having roughly similar soot mass at the vicinity of cake filtration onset as shown in table 4.1.
The cause of the difference then shall be attributed to the difference in the characteristic of the soot produced by both cycles. Principal Component Analysis (PCA) is then performed to analyze the data further to identify whether the driving cycles– FTP and LLC–tend to have a considerable differences in variables that are linked to particulate microcharacteristics.

4.2.1 PCA analysis

PCA can be described as a dimensionality reduction technique that aims to find a set of orthogonal principal components that maximize variances between the variables. Given a centred and standardized matrix X, with singular vector decomposition, it can be decomposed into:

$$X \approx \hat{X} = U_k \Sigma_k V_k^T \tag{4.1}$$

Where $\hat{X}$ is the approximation of the actual X and k is the choice of the number of principal components. The matrix $U_k\Sigma_k$ represents the score matrix and V_k^T is the principal component.

The variables chosen for the PCA are the ones that correlate to the soot particle emission based on the literature study. Torque and engine speed are chosen to represent the low-load and high-load characteristics of the cycles and they have influence in the particle microcharacteristics [43]. [44, 45] shows that advancing injection timing and pressure have a role in the particle diameter size and [46] shows that the start of injection crank angle has a correlation with the amount of soot produced. [47] shows that the gap between the pilot injection and the main injection affects the amount of NOx and soot emission as shown in [48] as well and it is linked to the soot-NOx tradeoff. The oxygen concentration in a cylinder in this case is represented by lambda which can be defined as the ratio of the air-fuel ratio to the stoichiometric equivalent of it. A higher amount of oxygen in a cylinder promotes in-cylinder soot oxidation which reduces the amount of soot emission [49].

Variable	Unit
Lambda	-
Start of Injection	deg
End of injection	deg
Separation pilot-main	deg
Torque	Nm
Engine speed	RPM
Engine-out exhaust gas temperature	degC
Engine-out NOx concentration	ppm
Rail pressure	Pa
Time idling	s

Table 4.2: Variables chosen for the PCA analysis

The X matrix is then defined with the aggregation values of those chosen variables on a window of 2 minutes of data. The data used for the PCA is the FTP loading case and LLC loading case up to the second weighing of the DPF such that the difference in the amount of data is smaller. The aggregation function chosen is mean except for the "time idling" variable which is aggregated based on the total time idling during that period. The goal of this analysis is not to compare them magnitude-wise, but to compare the difference between the different driving cycles as explained before. The results are as follows:

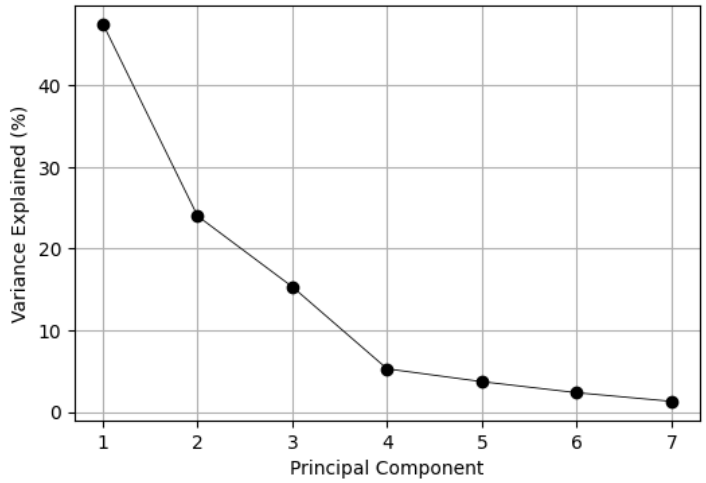

Figure 4.8: Scree plot of the PCA

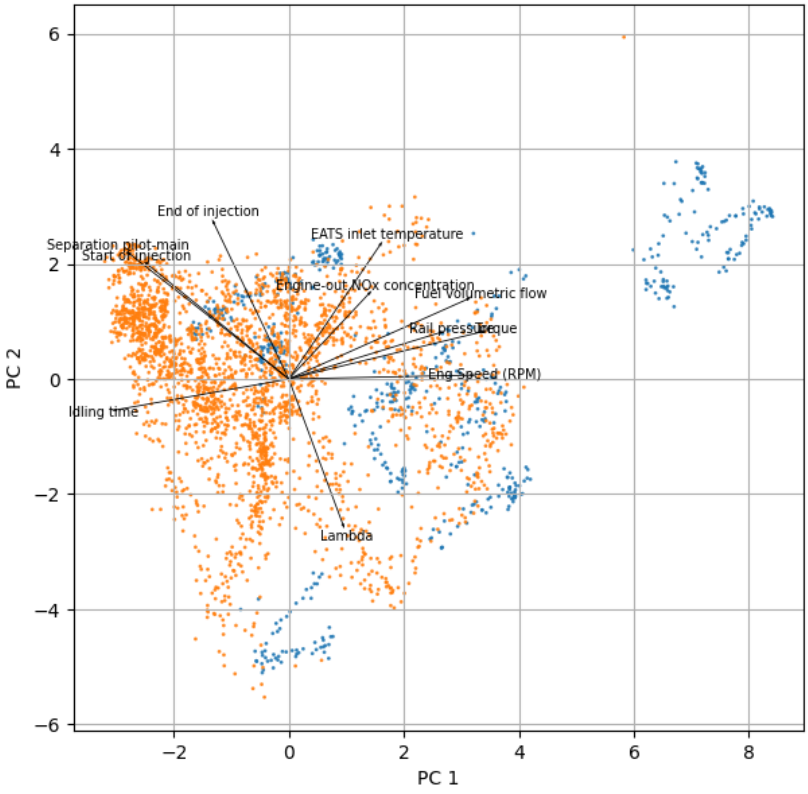

Figure 4.9: η The biplot of the PCA. Orange and blue dots represent LLC and FTP cases respectively-

In figure 4.9 we can see that there are separations between the driving cycles. Investigating this further would require looking at the soot deposition mechanism and its effect towards the permeabilities and subsequently the pressure drop. Through an experiment that was done by Choi and Lee in [36], it is known that in the deposi-

tion process, the soot particles starts to fill the porous DPF wall before forming soot cake. This phase represents the steep increase in pressure drop before it becomes relatively linear as previously mentioned. Research by Rakovec et.al [41] shows that soot cake has a small contribution towards the overall permeability drop and deep bed filtration plays a much larger role. Therefore, the latter defines the permeability throughout the entire loading process. Moreover, [41] also shows that the pressure drop during deep-bed loading and soot cake formation is dictated by the particle characteristics, which affect the depths of the wall penetration and packing densities. By linking these findings along with the fact that the difference lies only in the driving cycle, it can be considered highly probable that the LLC and FTP cycles indeed produce different soot particle characteristics that cause different behaviour of pressure drop.

Based on the PCA result, we can infer that in general, FTP has a relatively higher rail pressure, engine speed, and torque compared to LLC while the lambda does not produce a visually significant difference. LLC cycles however, has a slight difference toward the FTP with later start and end of injection, higher separation between pilot and main injection, as well as more time spent idling. By linking these findings to other findings from the literature, we can infer that FTP might have a lower particle diameter compared to LLC.

Higher engine speed causes shorter particle residence time which slows down particle surface growth [45, 50]. Earlier injection timing would primarily promotes better fuel-air mixing. However, according to study by Wang et.al in [45] showed that the effect of injection timing to particle size are complex. An increase in rail pressure also shows a reduction in the particle's primary diameter as shown by several results summarized in [45]. Idling might also produce higher HC emission and have an impact on PM generation as shown in [51, 52, 53]. The aforementioned hypothesis, however, is hard to prove when no measurement is made because soot generation is generally complex and different engine might cause different behaviours as well. Furthermore, by linking this finding into table 4.1 and the work by [54], DPF efficiency with different particle sizes might also affect the onset of cake filtration. If the hypothesis is right, then it might also due to the fact that the particle sizes produced by FTP happen to be filtered less efficiently compared to the LLC particle counterparts. Other factors such as the soot cake density, composition, permeability, and the depth of penetration of the particles towards the porous wall might also play a role though it is difficult to prove with the available data. The important point to make in this discussion is that the behaviour of DPF pressure drop is not only affected by the soot mass. It is also affected by the microstructural properties of the

soot particles, which in this study arguments have been made to link this difference to the particle size. Furthermore, Eastwood in [1] mentioned that during low load where the combustion temperature is generally lower, soot-forming reactions could be interrupted which leads to higher organic fractions in the particulate emission. It is indeed important to prove this hypothesis by taking a closer look at the particle by performing particle size distribution measurement as one example. However, due to the limitations of the thesis, the particle characteristics will be implied only by the comparison of PCA result.

4.3 Regenerative case

The regenerative case is represented by modes 2,4, and 5 with more emphasis in mode 4. An interesting takeaway from the regenerative case is that in figure 3.8, we can clearly see the hysteretical behavior of the soot mass with respect to the pressure drop represented by η. Although the real soot mass decrease during regeneration might not be linear, we can see that at the end of the regeneration, the value of η at the same weight is different from the loading case. According to observations by Choi et.al in [55], regenerations typically begin by oxidation of the soot within the porous wall. Therefore rapidly increasing the permeability and lowering the pressure drop. However, if the regeneration is not complete, then there might be soot cake still present within the inlet channel wall. A study by [56] et.al shows a similar observation. They also showed that the soot packing density after regeneration is lower than after loading. Figure 4.10 by [57] illustrates how the cake layer progresses during regeneration. In their conceptual model, a large pore opening occurs during regeneration which causes a decrease in pressure drop during regeneration.

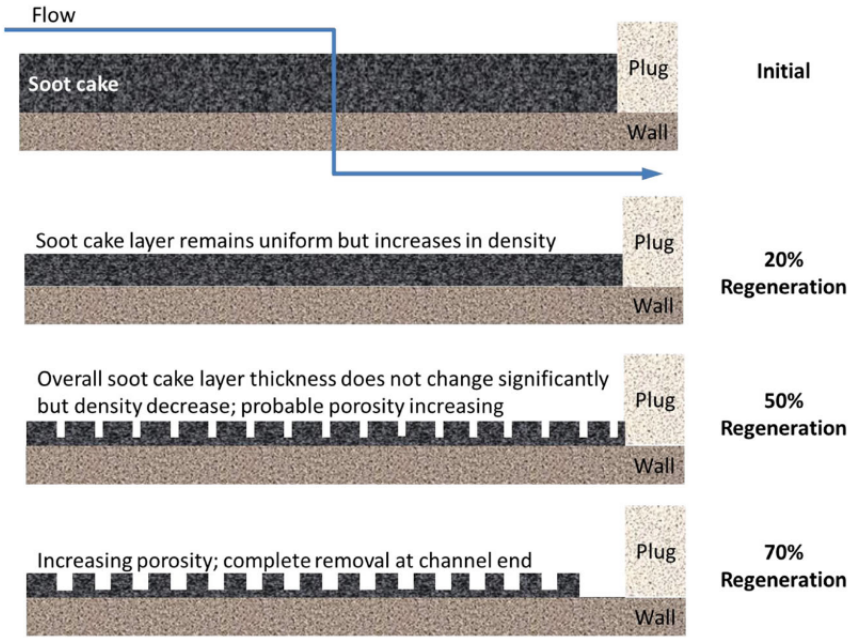

Figure 4.10: Illustration from [57]. Changes in the soot cake layer during regeneration

4.4 On the estimation of DPF particulate load with pressure difference

Previous sections have shown that estimating soot load using pressure drop sensor is not an easy task. Pressure drop across a DPF is actually caused by multiple things. It is an effect of many things, instead of being the one that affects the DPF. By evaluating multiple literatures, we can come up with the following simplified illustration of things that affect the pressure drop:

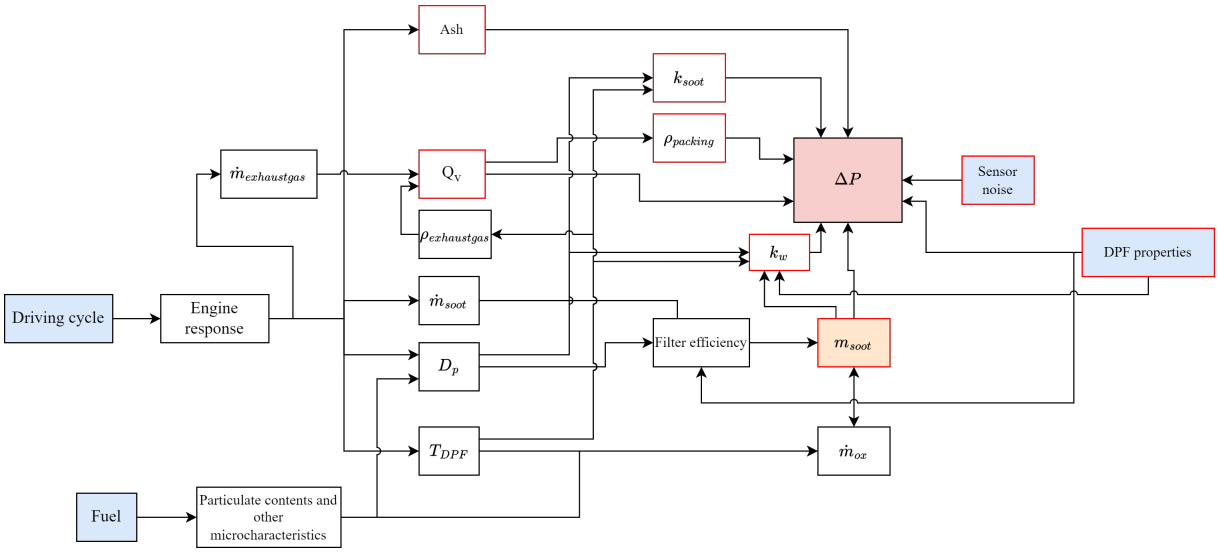

Figure 4.11: Illustration of things that affect pressure drop and soot mass deposit.

First and foremost, the pressure drop is directly affected by the variables with red borders. It is derived based on the equation by Konstandopoulos in (2.9). Pressure drop readings is also affected by the sensor noise, and volumetric flow, as well as dictated by the DPF properties as different DPF properties renders different pressure drop in clean state and deep-bed filtration stage [58]. An important step in the derivation of (2.9) as written in [37] involves expressing the velocity through the inlet and outlet channel through flow velocity and it is a function of the channel dimension. The volumetric flow velocity in itself is a function of the exhaust gas mass flow as well as the gas temperature if we refer to the ideal gas equation. Although the growth is slow, ash deposits have a complex effect on the behaviour of the pressure drop and it is well studied in [3, 18, 33, 34, 59]. In general, deposits of ash will affect the gradient of pressure drop concerning soot mass, rendering the pressure drop more sensitive to the addition of soot [35]. Meanwhile, in certain situations, ash may also block the DPF pore such that there is no soot deposit within the wall, hence making the pressure drop act in a way of soot cake filtration only. The soot cake permeability k_{soot} in itself is also a complex thing and cannot be easily estimated. Konstandopoulos in [23] expressed that the cake soot permeability correlates with the peclet number and can be calculated as a function of primary particle diameter, stoke-cunningham factor, and kuwabara factor. Haralampous in [60] on the other hand, proposed that the soot cake permeability is a function of local pressure and temperature, as mentioned in [61] as well. Lapuerta in [62] estimates the soot cake permeability by a function of its porosity and grain size. These models however, require assumptions of the aforementioned parameters. Porous wall permeability k_w

is a function of the DPF properties, as it is defined by the properties of the porous wall [63]. As soot deposits fill the porous wall, k_w will decrease up to the point where soot cake filtration happens [25]. $\rho_{loading}$ can be expressed as a function of the soot innate density and the porosity of the cake layer. [23] argues that the porosity can be estimated as a function of the Peclet number. Lapuerta in [62] shows that the porosity can evolve over time and it is a function of the amount of soot within the cake layer and the pores. Finally, it is also obvious that the amount of soot deposit will affect the pressure drop as it will constrict the flow through the pores, and channel, and increase friction in the flow [37].

Filter efficiency plays a huge role in determining which particle would get trapped. [16] shows that there are different efficiencies for each particle sizes. Chiavola et.al through their work in [54] and [64] also show the same thing. While the filtration efficiency is almost 100% during cake filtration, the type of particle that fills the porous wall will dictate the pressure drop behavior as observed by [41].

This entire relation of the aforementioned variables are more complex with regeneration. The oxidation of the soot particle will depend ultimately on the presence of oxygen, nitrogen oxides, and temperature as it provides the activation energy required for the oxidation. The presence of a catalyzed wall will reduce the required activation energy and possibly initiate a continuously regenerating trap. Typically, regeneration will oxidise the soot particles in the porous wall first before oxidizing the soot cake [36]. Bagi et.al in [18] shows that the regeneration strategy will affect the existing ash deposit and possibly develop an ash bridge or ash plugs. The rate of oxidation itself is dictated by the reactivity of the soot deposit [65].

Ultimately, these variables are dictated by the engine response which is dictated by the driving cycle or the driving condition itself and fuel type as mentioned in [66]. As explained in the previous chapter, soot formation is a complex process in itself. It is a challenging aspect to have a pinpoint accuracy of the particle characteristics. In this regard, the author did not say that it is impossible to estimate DPF particulate load based on pressure difference. In fact, it is one of the simplest and widely used methods to estimate the DPF soot load. However, achieving high accuracy is challenging despite the importance of heavy-duty diesel applications where fuel economy is of the upmost importance. Furthermore, the regeneration method affects the deposits which ultimately would make it possible to break any assumptions of pressure drop behavior if not accounted for. An accurate pressure drop-based particulate estimation must account for multiple other things that affect pressure drop readings as shown in figure 4.11.

In a hypothetical case where pressure drop-based estimation is used 100% of the

time, the author argued that the estimation will resemble those in the calibration map. The pressure drop calibration map should be based on the typical soot micro-characteristics condition that the calibration map is used in. The "switching" logic between the pressure drop-based estimation and model-based estimation should also consider whether the situation is roughly similar to the situation during the calibration or not.

4.5 Possible usage of pressure difference sensor

With the possibility of estimating normalized pressure drop η in real-time using recursive-least squares, the author proposes several possible usages of η in real driving scenarios other than particulate load estimation. The arguments proposed are not tested within this thesis. Therefore, further verification is required in future work.

4.5.1 Soot-free DPF verification

By looking at equation (2.9), we can see that when the DPF is empty of soot, η will only be a function of the clean wall permeability. If the clean wall permeability at different level of ash is well calibrated, then a DPF empty of soot, an indication of a complete regeneration, can be inferred based on the value of clean η as well as an estimate of the amount of ash itself.
This opens up a possibility to have different pressure drop calibration map where the difference lies in the amount of ash deposits. [33] shows that different amount of ash deposits will give different behavior of pressure drop with respect to particulate mass deposit. Therefore, if the amount of ash can be estimated and the corresponding pressure drop calibration map exist, the amount of soot deposit will be the estimated particulate load subtracted by the estimated ash amount.

4.5.2 DPF fault detection

By evaluating equation 2.9, we know that the pressure drop is not just a function of the flow condition and deposits but also a function of the geometry of the DPF. Therefore, if the pressure drop represented by η is having very sudden changes and went into values that are outside the typical values, mechanical failure within the DPF might occur.

4.5.3 Regeneration strategy

From the operational point of view, the existence of DPF is detrimental. Particulates gets trapped within the DPF, increases the exhaust backpressure, and in the end reduces the fuel efficiency [67]. As described in previous sections, regeneration serves as a way to oxidize the soot particulates such that the pressure drop reduces. Regeneration process however, relies on favorable conditions such as high DPF temperature to start. Depending on the strategy, in general increasing DPF temperature requires higher fuel consumption.

With this argument, we can see the conflict that arises. A strict regeneration strategy with more frequent regeneration will maintain a lower pressure drop throughout the operation with the expense of more fuel consumption due to regeneration. On the other hand, a more relaxed regeneration strategy reduces the regeneration fuel consumption while possibly having to operate with a higher particulate load and with a lower efficiency due to higher exhaust back pressure. The trade-off will be highly dependant on the vehicle itself and the use-case. However, if lower pressure drop is the one that is the most optimal, author argued that the regeneration strategy can be based on monitoring η instead of particulate mass.

5

Conclusion, suggestions, and Future Work

The conclusions of this thesis are as follow:

1. A comparison between the default estimation and the interpolated particulate mass has been made. A method to normalize pressure drop in real-time situations has also been proposed.
2. It is shown that an accurate and precise particulate mass estimation of DPF using pressure drop is a challenging task. Figure 3.8 shows that a hysteresis-like phenomenon occurs between the normalized pressure drop η and the interpolated particulate mass during loading and regeneration with different driving cycles. A literature-based inference has been done to identify the cause. It is hypothesized that the difference is mainly due to differences in particle size distributions although validation of this hypothesis was not done due to the limitation of this thesis.
3. Pressure drop across a DPF is an effect of various things and the amount of the particulate deposit is one of them. Therefore, a good estimation and/or assumption of various other things that affect the pressure drop is required to improve the inference of m_{soot} based on pressure drop. This is illustrated in figure 4.11.
4. Scania's default estimation is able to approximate the particulate loading to a considerable accuracy during the FTP loading and LLC loading case as shown in figure 3.4 and 4.2. We can say that the decision regarding the switching between pressure drop-based and model-based that is made by the default estimation system works well. With this, the author argued that if the pressure drop-based model needs to be improved, it shall start with calibrating a calibration map that matches well with the micro characteristics of the soot during the vehicle operation. Furthermore, The effect of ash needs to be accounted for.
5. The Author suggested three potential uses of pressure difference sensors along

with real-time estimation of η: Soot-free DPF verification, DPF fault detection, and as a basis in determining regeneration strategy. Further tests are needed to verify the applicability of these suggestions.

6. A Study on the micro-characteristics of the engine-out particulates needs to be done in concordance with the evaluation of filter performance and the development of a soot load estimator. This is because one of the most important metrics of filter performance–pressure drop–is highly affected by the particulates' micro-characteristics.

   This thesis also showed the possibility of performing real-time normalization of pressure drop through the usage of recursive least-squares. In regard to DPF particulate load estimation, as shown in this thesis, it can be done through an empirical approach such as the pressure drop-based estimation. The empirical model is often feasible for real-truck driving scenarios as it does not require extensive computational power. A very accurate non-empirical model-based approach, however, would require high computational power as it might involves multiple steps with multiple numbers of species [1]. For future efforts in particulate load estimation, the author argued that one of the best ways possible might be to develop a semi-empirical model, not an entirely empirical model. This approach can be developed by identifying the relation between engine modes and the particulate micro characteristics specifically for the engine and aftertreatment system in question as well as studying the evolution of soot particulate microcharacteristics inside the DPF. It might be possible then to develop multiple calibration maps in which the usage is based on a "proxy" variable representing particulate characteristics.

Bibliography

[1] Peter Eastwood. *Particulate emissions from vehicles*. Wiley-professionnal engineering publishing series. Chichester (G. B.): J. Wiley & Sons, 2008. ISBN: 978-0-470-72455-2.

[2] Dale R. Tree and Kenth I. Svensson. "Soot processes in compression ignition engines". In: *Progress in Energy and Combustion Science* 33.3 (June 2007), pp. 272–309. ISSN: 03601285. DOI: 10.1016/j.pecs.2006.03.002.

[3] Jianbin Luo. "Effect of regeneration method and ash deposition on diesel particulate filter performance: a review". In: *Environmental Science and Pollution Research* (2023).

[4] John Kasab and Andrea Strzelec. *Automotive Emissions Regulations and Exhaust Aftertreatment Systems*. SAE International, Aug. 31, 2020. ISBN: 978-0-7680-9955-3. DOI: 10.4271/9780768099560.

[5] John B. Heywood. *Internal combustion engine fundamentals*. Second revised edition. McGraw-Hill series in mechanical engineering. New York Chicago San Francisco [und 9 andere]: McGraw-Hill Education, 2018. 1028 pp. ISBN: 978-1-260-11610-6.

[6] Kazuhiro Akihama et al. "Mechanism of the Smokeless Rich Diesel Combustion by Reducing Temperature". In: SAE 2001 World Congress. Mar. 5, 2001, pp. 2001–01–0655. DOI: 10.4271/2001-01-0655.

[7] Anders Westlund. *Measuring and Predicting Transient Diesel Engine Emissions*. Backup Publisher: KTH, Machine Design (Div.) ISSN: 1400-1179 Issue: 2009:07 Pages: 53 Series: Trita-MMK. 2009.

[8] Zibin Yin et al. "A review of the development and application of soot modelling for modern diesel engines and the soot modelling for different fuels". In: *Process Safety and Environmental Protection* 178 (Oct. 2023), pp. 836–859. ISSN: 09575820. DOI: 10.1016/j.psep.2023.08.075.

[9] Alexander Sappok and Victor W. Wong. "Lubricant-Derived Ash Properties and Their Effects on Diesel Particulate Filter Pressure-Drop Performance".

In: *Journal of Engineering for Gas Turbines and Power* 133.3 (Mar. 1, 2011), p. 032805. ISSN: 0742-4795, 1528-8919. DOI: 10.1115/1.4001944.

[10] W. L. Easley, A. M. Mellor, and T. P. Gardner. "Flame Temperature Correlation of Emissions from Diesels Operated on Alternative Fuels". In: International Spring Fuels & Lubricants Meeting. May 7, 2001, pp. 2001–01–2014. DOI: 10.4271/2001-01-2014.

[11] Xiangang Wang et al. "Diesel engine gaseous and particle emissions fueled with diesel–oxygenate blends". In: *Fuel* 94 (Apr. 2012), pp. 317–323. ISSN: 00162361. DOI: 10.1016/j.fuel.2011.09.016.

[12] Avinash Kumar Agarwal et al. "Effect of fuel injection timing and pressure on combustion, emissions and performance characteristics of a single cylinder diesel engine". In: *Fuel* 111 (Sept. 2013), pp. 374–383. ISSN: 00162361. DOI: 10.1016/j.fuel.2013.03.016.

[13] T. Thurnheer et al. "Experimental investigation on different injection strategies in a heavy-duty diesel engine: Emissions and loss analysis". In: *Energy Conversion and Management* 52.1 (Jan. 2011), pp. 457–467. ISSN: 01968904. DOI: 10.1016/j.enconman.2010.06.074.

[14] Athanasios Dimitriadis et al. "Evaluation of a Hydrotreated Vegetable Oil (HVO) and Effects on Emissions of a Passenger Car Diesel Engine". In: *Frontiers in Mechanical Engineering* 4 (July 31, 2018), p. 7. ISSN: 2297-3079. DOI: 10.3389/fmech.2018.00007.

[15] Euijoon Shim, Hyunwook Park, and Choongsik Bae. "Comparisons of advanced combustion technologies (HCCI, PCCI, and dual-fuel PCCI) on engine performance and emission characteristics in a heavy-duty diesel engine". In: *Fuel* 262 (Feb. 2020), p. 116436. ISSN: 00162361. DOI: 10.1016/j.fuel.2019.116436.

[16] E. Ohara et al. "Filtration Behavior of Diesel Particulate Filters (1)". In: SAE World Congress & Exhibition. Apr. 16, 2007, pp. 2007–01–0921. DOI: 10.4271/2007-01-0921.

[17] José Ramón Serrano et al. "Filtration modelling in wall-flow particulate filters of low soot penetration thickness". In: *Energy* 112 (Oct. 2016), pp. 883–898. ISSN: 03605442. DOI: 10.1016/j.energy.2016.06.121.

[18] Sujay Bagi, Nishant Singh, and Rob Andrew. "Investigation into Ash from Field Returned DPF Units: Composition, Distribution, Cleaning Ability and DPF Performance Recovery". In: SAE 2016 World Congress and Exhibition. Apr. 5, 2016, pp. 2016–01–0928. DOI: 10.4271/2016-01-0928.

[19] Alexander Sappok and Victor W. Wong. “Lubricant-Derived Ash Properties and Their Effects on Diesel Particulate Filter Pressure Drop Performance”. In: *ASME 2009 Internal Combustion Engine Division Fall Technical Conference*. ASME 2009 Internal Combustion Engine Division Fall Technical Conference. Lucerne, Switzerland: ASMEDC, Jan. 1, 2009, pp. 327–343. ISBN: 978-0-7918-4363-5 978-0-7918-3858-7. DOI: 10.1115/ICEF2009-14080.

[20] Chung Ting Lao, Jethro Akroyd, and Markus Kraft. “Modelling treatment of deposits in particulate filters for internal combustion emissions”. In: *Progress in Energy and Combustion Science* 96 (May 2023), p. 101043. ISSN: 03601285. DOI: 10.1016/j.pecs.2022.101043.

[21] Athanasios G. Konstandopoulos and John H. Johnson. “Wall-Flow Diesel Particulate Filters—Their Pressure Drop and Collection Efficiency”. In: SAE International Congress and Exposition. Feb. 1, 1989, p. 890405. DOI: 10.4271/890405.

[22] Athanasios G. Konstandopoulos, Evangelos Skaperdas, and Mansour Masoudi. “Inertial Contributions to the Pressure Drop of Diesel Particulate Filters”. In: SAE 2001 World Congress. Mar. 5, 2001, pp. 2001–01–0909. DOI: 10.4271/2001-01-0909.

[23] Athanasios G. Konstandopoulos, Evangelos Skaperdas, and Mansour Masoudi. “Microstructural Properties of Soot Deposits in Diesel Particulate Traps”. In: SAE 2002 World Congress & Exhibition. Mar. 4, 2002, pp. 2002–01–1015. DOI: 10.4271/2002-01-1015.

[24] Mansour Masoudi et al. “Validation of a Model and Development of a Simulator for Predicting the Pressure Drop of Diesel Particulate Filters”. In: SAE 2001 World Congress. Mar. 5, 2001, pp. 2001–01–0911. DOI: 10.4271/2001-01-0911.

[25] Boopathi S. Mahadevan, John H. Johnson, and Mahdi Shahbakhti. “Predicting Pressure Drop, Temperature, and Particulate Matter Distribution of a Catalyzed Diesel Particulate Filter Using a Multi-Zone Model Including Cake Permeability”. In: *Emission Control Science and Technology* 3.2 (June 2017), pp. 171–201. ISSN: 2199-3629, 2199-3637. DOI: 10.1007/s40825-017-0062-6.

[26] Christopher Depcik, Bailey Spickler, and Anmesh Gaire. “Revisiting the Single Equation Pressure Drop Model for Particulate Filters”. In: *SAE Int. J. Engines* 11 (2018).

[27] M. Schejbal et al. “Modelling of soot oxidation by NO 2 in various types of diesel particulate filters”. In: *Fuel* 89.9 (Sept. 2010), pp. 2365–2375. ISSN: 00162361. DOI: 10.1016/j.fuel.2010.04.018.

[28] Qu Dawei. “Research on particulate filter simulation and regeneration control strategy”. In: *Mechanical Systems and Signal Processing* (2017).

[29] Fuwu Yan, Zhizhou Cai, and Jie Hu. “The state-of-the-art of soot load estimation in diesel particulate filters: A review”. In: *E3S Web of Conferences* 268 (2021). Ed. by F. Yan et al., p. 01021. ISSN: 2267-1242. DOI: 10.1051/e3sconf/202126801021.

[30] Tae Joong Wang. “A methodology for estimating the permeability of a soot deposit in a wall-flow diesel particulate filter”. In: *Proceedings of the Institution of Mechanical Engineers, Part D: Journal of Automobile Engineering* 228.10 (Sept. 2014), pp. 1154–1169. ISSN: 0954-4070, 2041-2991. DOI: 10.1177/0954407013504390.

[31] De-yuan Wang et al. “Novel soot loading prediction model of diesel particulate filter based on collection mechanism and equivalent permeability”. In: *Fuel* 286 (Feb. 2021), p. 119409. ISSN: 00162361. DOI: 10.1016/j.fuel.2020.119409.

[32] Dongwei Yao et al. “Research on dynamic modeling and carbon load estimation of diesel particulate filter”. In: *Energy Sources, Part A: Recovery, Utilization, and Environmental Effects* 45.4 (Oct. 2, 2023), pp. 12165–12180. ISSN: 1556-7036, 1556-7230. DOI: 10.1080/15567036.2023.2269126.

[33] Alexander Sappok and Victor W. Wong. “Ash Effects on Diesel Particulate Filter Pressure Drop Sensitivity to Soot and Implications for Regeneration Frequency and DPF Control”. In: *SAE International Journal of Fuels and Lubricants* 3.1 (Apr. 12, 2010), pp. 380–396. ISSN: 1946-3960. DOI: 10.4271/2010-01-0811.

[34] Alexander Sappok et al. “Characteristics and Effects of Ash Accumulation on Diesel Particulate Filter Performance: Rapidly Aged and Field Aged Results”. In: SAE World Congress & Exhibition. Apr. 20, 2009, pp. 2009–01–1086. DOI: 10.4271/2009-01-1086.

[35] Nishant Singh and Silpa Mandarapu. “DPF Soot Estimation Challenges and Mitigation Strategies and Assessment of Available DPF Technologies”. In: SAE 2013 World Congress & Exhibition. Apr. 8, 2013, pp. 2013–01–0838. DOI: 10.4271/2013-01-0838.

[36] Seungmok Choi and Kyeong Lee. “Detailed Investigation of Soot Deposition and Oxidation Characteristics in a Diesel Particulate Filter Using Optical Visualization”. In: SAE 2013 World Congress & Exhibition. Apr. 8, 2013, pp. 2013–01–0528. DOI: 10.4271/2013-01-0528.

[37] Athanasios G. Konstandopoulos et al. “Fundamental Studies of Diesel Particulate Filters: Transient Loading, Regeneration and Aging”. In: SAE 2000 World Congress. Mar. 6, 2000, pp. 2000–01–1016. DOI: 10.4271/2000-01-1016.

[38] Zhizhou Cai et al. “Lumped model for evaluating dynamic filtration and pressure drop behaviour in diesel particulate filters”. In: *Fuel* 365 (June 2024), p. 131311. ISSN: 00162361. DOI: 10.1016/j.fuel.2024.131311.

[39] Torsten Söderström and Petre Stoica. *System identification*. Prentice Hall International series in systems and control engineering. New York: Prentice Hall, 1989. 612 pp. ISBN: 978-0-13-881236-2.

[40] Karl J. Åström and Björn Wittenmark. *Adaptive control*. 2. ed. Mineola, N.Y: Dover Publ, 2008. 573 pp. ISBN: 978-0-486-46278-3.

[41] Nicholas Rakovec, Sandeep Viswanathan, and David E. Foster. “Micro-scale Study of DPF Permeability as a Function of PM Loading”. In: *SAE International Journal of Engines* 4.1 (Apr. 12, 2011), pp. 913–921. ISSN: 1946-3944. DOI: 10.4271/2011-01-0815.

[42] Athanasios G. Konstandopoulos and Rozina Metallinou. “Parametric Representation of the Entire Pressure Drop Evolution during Particulate Filter Loading”. In: *SAE International Journal of Advances and Current Practices in Mobility* 2.5 (Apr. 14, 2020), pp. 3017–3023. ISSN: 2641-9645. DOI: 10.4271/2020-01-1433.

[43] Zi Xiu Wang, Q. Peter He, and Jin Wang. “Comparison of variable selection methods for PLS-based soft sensor modeling”. In: *Journal of Process Control* 26 (Feb. 1, 2015), pp. 56–72. ISSN: 0959-1524. DOI: 10.1016/j.jprocont.2015.01.003.

[44] Urs Mathis et al. “Influence of Diesel Engine Combustion Parameters on Primary Soot Particle Diameter”. In: *Environmental Science & Technology* 39.6 (Mar. 1, 2005), pp. 1887–1892. ISSN: 0013-936X, 1520-5851. DOI: 10.1021/es049578p.

[45] Xiaochen Wang et al. “An overview of physical and chemical features of diesel exhaust particles”. In: *Journal of the Energy Institute* 92.6 (Dec. 2019), pp. 1864–1888. ISSN: 17439671. DOI: 10.1016/j.joei.2018.11.006.

[46] Haifeng Liu et al. “Study of the control strategies on soot reduction under early-injection conditions on a diesel engine”. In: *Fuel* 139 (Jan. 2015), pp. 472–481. ISSN: 00162361. DOI: 10.1016/j.fuel.2014.09.011.

[47] Seuk Cheun Choi et al. “Effects of Fuel Injection Parameters on the Morphological Characteristics of Soot Particulates and Exhaust Emissions from a

Light-Duty Diesel Engine". In: *Energy & Fuels* 24.5 (May 20, 2010), pp. 2875–2882. ISSN: 0887-0624, 1520-5029. DOI: 10.1021/ef901561u.

[48] S. Narayan, Sasa Milojevic, and Vipul Gupta. "Combustion monitoring in engines using accelerometer signals". In: *Journal of Vibroengineering* 21.6 (Sept. 30, 2019), pp. 1552–1563. ISSN: 1392-8716, 2538-8460. DOI: 10.21595/jve.2019.20516.

[49] Jiaqiang E et al. "Soot formation mechanism of modern automobile engines and methods of reducing soot emissions: A review". In: *Fuel Processing Technology* 235 (Oct. 2022), p. 107373. ISSN: 03783820. DOI: 10.1016/j.fuproc.2022.107373.

[50] A Neer and U Koylu. "Effect of operating conditions on the size, morphology, and concentration of submicrometer particulates emitted from a diesel engine". In: *Combustion and Flame* 146.1 (July 2006), pp. 142–154. ISSN: 00102180. DOI: 10.1016/j.combustflame.2006.04.003.

[51] Jun Cong Ge et al. "Effect of injection timing on combustion, emission and particle morphology of an old diesel engine fueled with ternary blends at low idling operations". In: *Energy* 253 (Aug. 2022), p. 124150. ISSN: 03605442. DOI: 10.1016/j.energy.2022.124150.

[52] J. S. Kinsey et al. "Characterization of Fine Particle and Gaseous Emissions during School Bus Idling". In: *Environmental Science & Technology* 41.14 (July 1, 2007), pp. 4972–4979. ISSN: 0013-936X, 1520-5851. DOI: 10.1021/es0625024.

[53] Wei Deng et al. "Primary particulate emissions and secondary organic aerosol (SOA) formation from idling diesel vehicle exhaust in China". In: *Science of The Total Environment* 593-594 (Sept. 2017), pp. 462–469. ISSN: 00489697. DOI: 10.1016/j.scitotenv.2017.03.088.

[54] Ornella Chiavola, Giancarlo Chiatti, and Nidal Sirhan. "Impact of Particulate Size During Deep Loading on DPF Management". In: *Applied Sciences* 9.15 (July 30, 2019), p. 3075. ISSN: 2076-3417. DOI: 10.3390/app9153075.

[55] Seungmok Choi, Kwang-Chul Oh, and Chun-Bum Lee. "The effects of filter porosity and flow conditions on soot deposition/oxidation and pressure drop in particulate filters". In: *Energy* 77 (Dec. 2014), pp. 327–337. ISSN: 03605442. DOI: 10.1016/j.energy.2014.08.049.

[56] D. Pinturaud et al. "Experimental Study of DPF Loading and Incomplete Regeneration". In: 8th International Conference on Engines for Automobiles. Sept. 16, 2007, pp. 2007–24–0094. DOI: 10.4271/2007-24-0094.

[57] Todd J. Toops et al. “Progression of Soot Cake Layer Properties During the Systematic Regeneration of Diesel Particulate Filters Measured with Neutron Tomography”. In: *Emission Control Science and Technology* 1.1 (Jan. 2015), pp. 24–31. ISSN: 2199-3629, 2199-3637. DOI: 10.1007/s40825-014-0008-1.

[58] Dong Tang et al. “Influence of Asymmetric Channel Structure on Capture and Regeneration Process of Diesel Particulate Filter”. In: *Emission Control Science and Technology* 9.3 (Dec. 2023), pp. 166–176. ISSN: 2199-3629, 2199-3637. DOI: 10.1007/s40825-023-00229-w.

[59] Kazuhiro Yamamoto and Takuya Morimoto. “Effects of Wall-Ash and Plug-Ash on Pressure Drop and Soot Deposition in Diesel Particulate Filter”. In: *Emission Control Science and Technology* 8.3 (Dec. 2022), pp. 122–137. ISSN: 2199-3629, 2199-3637. DOI: 10.1007/s40825-022-00214-9.

[60] O. A. Haralampous et al. “Diesel particulate filter pressure drop Part 2: On-board calculation of soot loading”. In: *International Journal of Engine Research* 5.2 (Apr. 1, 2004), pp. 163–173. ISSN: 1468-0874, 2041-3149. DOI: 10.1243/146808704773564569.

[61] Willard W. Pulkrabek and Warren E. Ibele. “The effect of temperature on the permeability of a porous material”. In: *International Journal of Heat and Mass Transfer* 30.6 (June 1987), pp. 1103–1109. ISSN: 00179310. DOI: 10.1016/0017-9310(87)90040-8.

[62] Magín Lapuerta, Fermín Oliva, and Simón Martínez-Martínez. “Modeling of the Soot Accumulation in DPF Under Typical Vehicle Operating Conditions”. In: *SAE International Journal of Fuels and Lubricants* 3.2 (Oct. 25, 2010), pp. 532–542. ISSN: 1946-3960. DOI: 10.4271/2010-01-2097.

[63] Kazuhiro Yamamoto and Tatsuya Sakai. “Effect of Pore Structure on Soot Deposition in Diesel Particulate Filter”. In: *Computation* 4.4 (Dec. 2, 2016), p. 46. ISSN: 2079-3197. DOI: 10.3390/computation4040046.

[64] Ornella Chiavola et al. “Modeling of Soot Deposition and Active Regeneration in Wall-flow DPF and Experimental Validation”. In: SAE Powertrains, Fuels & Lubricants Meeting. Sept. 15, 2020, pp. 2020–01–2180. DOI: 10.4271/2020-01-2180.

[65] Kuen Yehliu et al. “Impact of engine operating modes and combustion phasing on the reactivity of diesel soot”. In: *Combustion and Flame* 160.3 (Mar. 2013), pp. 682–691. ISSN: 00102180. DOI: 10.1016/j.combustflame.2012.11.003.

[66] María Abián et al. “Interaction of diesel engine soot with NO2 and O2 at diesel exhaust conditions. Effect of fuel and engine operation mode”. In: *Fuel*

212 (Jan. 2018), pp. 455–461. ISSN: 00162361. DOI: 10.1016/j.fuel.2017.10.025.

[67] Ingo Mikulic, Reggie Zhan, and Scott Eakle. "Dependence of Fuel Consumption on Engine Backpressure Generated by a DPF". In: SAE 2010 World Congress & Exhibition. Apr. 12, 2010, pp. 2010–01–0535. DOI: 10.4271/2010-01-0535.

[68] George E. P. Box. "Science and Statistics". In: *Journal of the American Statistical Association* 71.356 (Dec. 1976), pp. 791–799. ISSN: 0162-1459, 1537-274X. DOI: 10.1080/01621459.1976.10480949.

A

Appendix 1: On the estimation of η

A.1 Batch estimation

Estimation of η can be done more simply through ordinary least squares. The optimum η in a least-squares sense that fits equation 3.2 can be found by solving the following equation:

$$\eta_k = (X_k^T X_k)^{-1}(X_k^T y_k) \tag{A.1}$$

Where:

$$X_k = \begin{bmatrix} (Q_v\mu)_1 \\ (Q_v\mu)_2 \\ (Q_v\mu)_3 \\ (Q_v\mu)_4 \\ (Q_v\mu)_5 \\ (Q_v\mu)_6 \\ \vdots \\ (Q_v\mu)_n \end{bmatrix} \tag{A.2}$$

$$y_k = \begin{bmatrix} \Delta p_1 \\ \Delta p_2 \\ \Delta p_3 \\ \vdots \\ \Delta p_n \end{bmatrix} \tag{A.3}$$

One can see quite clearly the drawbacks of this method. The regression cannot be done to estimate η in real-time since it needs to accumulate measurements up until it reaches n measurement points. Hence the name batch estimation. The estimated η is then available only once per n measurements and n is a fixed-parameter.

A.2 The effect of update mechanism

Update mechanism refers to "when" the estimation of η is done. In the case of batch estimation, it refers to the condition in which the measurements are considered to be put into the matrix X_k and y_k. In RLS, it refers to condition in which the next step is done. While it may not seems to be significant at a glance, this has a profound effect on the value of the estimated η.
The update mechanism for batch estimation is illustrated in the following figure:

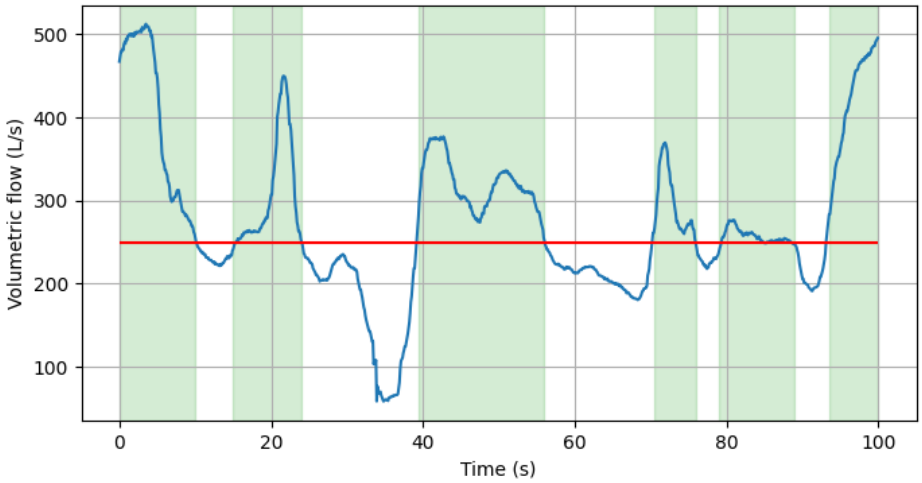

Figure A.1: Illustration of update mechanism for batch estimation

Suppose the update is set to occur when the volumetric flow through the DPF is above 250 l/s. This limit is illustrated as the red line in figure A.1. Periods where the data is considered for the estimation is highlighted in green. Therefore, each "window" of green highlight in the figure is considered as one k in equation (A.1). If for a single k the amount of datapoints exceed n, then that particular window is divided into multiple k such that no amount of data in a single k exceeds n.
Using the data from the LLC loading and regenerative case (mode 3+4), the η obtained from batch estimation are as follow:

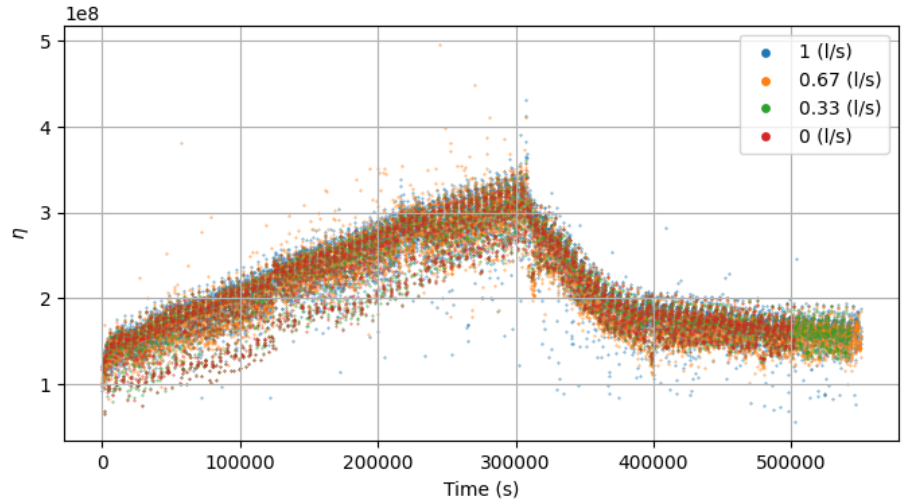

Figure A.2: Batch estimation of η. The color represent different volumetric flow threshold

As shown in the figure above, the estimation is relatively noisy. Savitsky-Golay filtering is then done and resulting in the following figure:

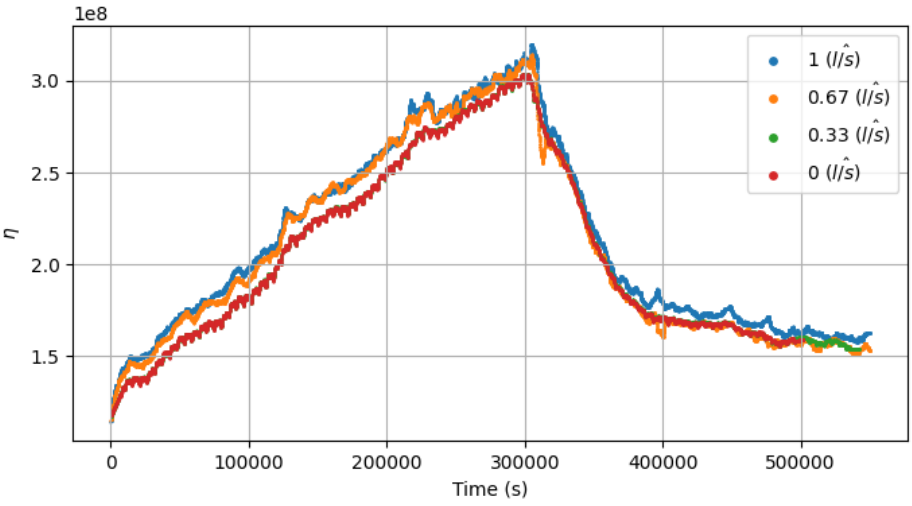

Figure A.3: Batch estimation η filtered with Savitsky-Golay. The color represent different volumetric flow threshold

We can see that diferent update mechanism produces different magnitude of η while to some extent preserves the general shape or trend of η. Now we turn our attention to the update mechanism of the RLS method. Since this is algorithm is supposed to be done in real-time, it reads the incoming stream of datapoints one-by-one. The update mechanism then refers to the condition in which the new estimation is made. Varying the volumetric flow update limit results in the following η result:

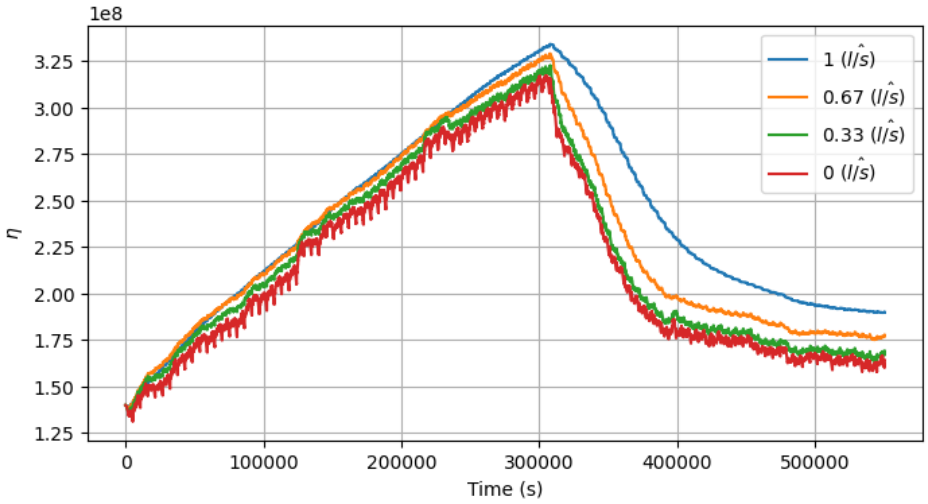

Figure A.4: Estimation of η with varying volumetric flow threshold. The color represent different volumetric flow update mechanism

There are noticeable differences in term of magnitude in a similar fashion to the batch estimation case.Table A.1 shows the comparison of the root-mean squared error of both batch estimation and RLS.

Q_v $(\frac{\hat{l}}{s})$	RLS	Batch estimation
0	0.55	0.48
0.33	0.61	0.47
0.67	0.64	0.56
1.00	1.00	0.54

Table A.1: Root mean squared error $(\hat{Pa})$ of different volumetric flow threshold in RLS and batch estimation

The root-mean squared error is in normalized term due to confidentiality. However, one can see that a more relaxed update mechanism tends to have lower error while having more noise as can be seen in the figures above. With these results, one must consider the update mechanism upon interpreting η in its numerical nature. While mathematically η can be defined as the first term in 2.9 without the volumetric flow Q_v and viscosity μ, the definition involves variables with very different magnitudes. As an example, the cell dimensions are typically within millimeter scale with 10^{-3} order in SI unit. The permeabilities on the other hand, are typically within the order of 10^{-12} to 10^{-14}. The η as we seen in previous chapters, are within the order of 10^{8}.

In this thesis, no exact numerical interpretation of η was made. The observation made in 4.1 shows the average value around several timesteps before and after the

observation point. Moreover, author would like to emphasize the infamous aphorism within the engineering world, "All models are wrong, but some are useful" as first coined by George P. Box in [68] . The pressure drop model presented by Konstandopoulos et.al as written in 2.9 is useful and has been used in many research within the topic of DPF. However, one must always remember that nature–in this context represented by the particulates behavior within the DPF–might behave differently from the model. In fact, many variations of the pressure drop model exist such as in [26]. This method might be able to exactly estimate the trends and conditions such as deep-bed filtration and cake filtration. However, one shall be very careful when trying to perform some numerical inference from η.
Further exploration regarding the estimation methods and pressure-drop models were not done within this thesis due to time limitation.

DEPARTMENT OF MECHANICAL AND MARITIME SCIENCES
CHALMERS UNIVERSITY OF TECHNOLOGY
Gothenburg, Sweden
www.chalmers.se

CHALMERS
UNIVERSITY OF TECHNOLOGY